3

Aerodynamic design of wind turbine rotors

C. BAK, Technical University of Denmark, Denmark

DOI: 10.1533/9780857097286.1.59

Abstract: This chapter describes the process of aerodynamic rotor design for horizontal axis wind turbines. Apart from describing the state-of-the-art, it presents the mathematical models used, explains how airfoil and rotor control choice are decided and lists common design constraints. An example is used to illustrate the rotor design process, covering all the main aspects from choice of rotor size, airfoil types and number of blades to the exact aerodynamic shape of the blades. At the end of the chapter there is a summary of future trends and sources of further information.

Key words: rotor design, wind turbine rotor, wind turbine airfoils, aerodynamic design, wind turbine power performance.

Note: This chapter is a revised and updated version of Chapter 6 'Aerodynamic design of wind turbine rotors' by C. Bak in *Wind energy systems*, edited by J. D. Sørensen and J. N. Sørensen, Woodhead Publishing Limited, 2010, ISBN: 978-1-84569-580-4.

3.1 Introduction

The wind turbine rotor with its blades is the part of the wind turbine that extracts kinetic energy from the wind and converts it into mechanical power and further into electricity, which can be used for water heating, pumping, etc. A result of extracting energy is that the speed of airflow through the area swept by the rotor is reduced in the rotor plane and behind the rotor. There are therefore many different ways to extract energy from the wind. Wind turbine rotors can be divided into those which are driven by the lift on the airfoils and those which are driven by the drag on the blades. In addition, rotors can be divided into those with low rotational speed, causing a high torque, and those with high rotational speed, which are common in electricity production. Furthermore, wind turbines can be divided into horizontal axis wind turbines (HAWTs) and vertical axis wind turbines (VAWTs). The most common today is the HAWT, see Fig. 3.1 (a), with varying numbers of blades, driven by the lift on the airfoils, and with high rotational speed. A VAWT is also shown, see Fig. 3.1 (b), driven by the lift on the airfoils and with high rotational speed. The three-bladed HAWT with the rotor upstream

(a)

(b)

3.1 (a) Horizontal axis wind turbine (HAWT), Siemens 2.3 MW wind turbine, 69 m hub height, situated at Rødsand, Denmark. (*Source*: Photo by Christian Bak, DTU Wind Energy.) (b) Vertical axis wind turbine (VAWT), Éole 4 MW wind turbine, height of 110 m, situated at Cap Chat, Quebec, Canada. (*Source*: Photo by Paul Gipe, wind-works.org.)

of the tower is the dominating concept of today, and the ten biggest suppliers of wind energy, installing around 78% of the capacity in 2011,[1] and the majority of remaining suppliers, use this concept. Because of the significant domination of the HAWT concept, this chapter will limit the description of aerodynamic design to HAWT rotors driven by the lift on the airfoils and with high rotational speed.

This chapter describes briefly the state-of-the-art within aerodynamic design of rotors and explains the principles of an aerodynamic design process that uses simple but common methods. The introduction to rotor design focusses on the Blade Element Momentum (BEM) method, and this is followed by an explanation of how decisions are reached concerning rotational speed, rotor size, rotor control and number of blades, what the design constraints are, and how the rotor design is evaluated. Based on this introduction, an example of a rotor design process, covering the design of the first draft of a rotor for a 1 MW wind turbine, is described. The methods for carrying out an aerodynamic rotor design are thus described, but that part of the process from the first draft design, as presented in this chapter, to the final rotor, including aeroelastic computations, structural considerations such as buckling and tip deflection, and the performance of the rotor in the wind turbine system, is not shown. At the end of the chapter, future trends and sources of further information can be found.

Although the scope of this chapter is restricted to aerodynamic rotor design it should be emphasized that the rotor design process should be considered as part of the wind turbine design process as a whole, which includes the aeroelastic response of the entire wind turbine and the structural design of the blades. Further, aerodynamic rotor design is closely connected to the process of structural lay-up of the blade and choice of material. This chapter's description of the aerodynamic rotor design process will therefore include occasional reminders to the reader of the importance of these connections.

3.1.1 State-of-the-art rotor design

Many simulation tools have been developed for prediction of wind turbine rotor flow. They range from the very simple models, such as the Blade Element Momentum (BEM) method, requiring low computational means, to the very advanced models, such as three-dimensional Computational Fluid Dynamics (CFD) which resolves the boundary layers on the rotor and the domain several rotor diameters upstream and downstream of the rotor plane, thus requiring high computational means. However, despite the fast development of computer power, using the very advanced models to produce predictions to inform the optimization process is, even now in 2013,

still rather time-consuming; these methods should therefore be considered as tools for evaluating the rotor design, rather than as part of the inherently iterative rotor design process.

That is the reason for the extensive use of the BEM method in tools designed to predict rotor aerodynamics, but also in tools for predicting the aeroelastic response of the entire wind turbine. A common way of designing rotors in 2013 is to produce a draft rotor design using a simple method such as the BEM method, and then evaluate it using a so-called aeroelastic code. If the rotor design turns out to be efficient, it can be evaluated using advanced tools, such as CFD, if they are available.

The rotor design approach described above is a manual process based on trial-and-error, and works with great success if the designer is experienced. However, the design can also be carried out using numerical optimization, where an object function is minimized or maximized. The object function could be the power coefficient or the annual energy production subject to constraints, such as maximum loads below a certain level, and absolute thickness distribution of the blades above a certain level to ensure a certain minimum stiffness. In such a tool, coupling to an aeroelastic code is possible, which can automate the rotor and wind turbine design to some degree. However, the output of such a design study is dependent on the object function and the constraints, so carrying out such a design process requires an experienced user. Furthermore, such a design method is time-consuming, especially if the design is based on aeroelastic calculations, and therefore certain simplifications are often needed to reduce the computational time. Despite being time-consuming, such a tool can be profitable, because trends in the rotor design, which are not part of the analysis, can be revealed. At least one tool can create designs based on both aerodynamic and aeroelastic calculations using numerical optimization.[2] If aerodynamic optimizations are sufficient, a few other tools can be used.[3]

Because the simple BEM method is often used in the rotor design process, the design could benefit from being evaluated using more advanced methods. The most time-consuming simulation method is based on an exact modeling of the surface geometry of the blade and rotor, where the boundary layer of the flow over the surface is resolved. Here, a significant part of the operator time is spent on generating a computational mesh that satisfies the conditions necessary for creating reliable solutions. Apart from commercially available CFD codes,[4–6] significant work has also been carried out since the start of the 1990s to develop this technique specifically for wind turbines.[7–10] Reduced models exist as well, where the rotor is modeled by introducing volume forces into the flow, either by lines simulating each blade (Actuator Line method),[11, 12] or by a disc simulating the entire rotor, where the blade forces are smeared out on the entire rotor plane (Actuator Disc method).[13] The results from these methods compare quite well with

the full model, as described above, where power curves and force distributions along the blades, for example, are very similar. However, details such as airfoil characteristics and tip flow cannot be extracted. Finally, techniques using discrete vortices have been developed and are fairly fast as well; this depends, however, on whether the wake behind the turbine is free to move or frozen.[14]

3.1.2 Models and elements used in the rotor design process

In the previous section it was stated that the most common method for prediction of rotor performance in the aerodynamic design of rotors was the Blade Element Momentum (BEM) method and that it required low computational means. In the sections that follow, the various elements required for the aerodynamic design of rotors using BEM are described. Because the aerodynamic rotor design should be considered as integrated in the design of the entire wind turbine, aspects such as constraints relating to the aerodynamic rotor design process, are described. Furthermore, a few rules of thumb required to make the rotor design process operational are described, but these rules are based on the experience of existing rotor designs and are not necessarily applicable for all designs.

3.2 The blade element momentum (BEM) method

The BEM method was developed in the 1930s,[15] and since then other, but not very different, formulations have been developed.[16–18] In what follows, the BEM method will be described, starting with a simplified model which assumes that the flow through the rotor behaves the same way at all points making the problem one-dimensional. Furthermore, the assumption in the one-dimensional problem is that the rotor has no losses such as friction caused by the air viscosity and no losses caused by the flow at the tips. The description of the simplified one-dimensional model is followed by a description of the more advanced BEM model, which uses the one-dimensional model in each annular element and also takes these types of losses into account.

3.2.1 One-dimensional momentum theory

In this first analysis of the rotor flow, it is assumed that the rotor is a disc and that it is ideal, i.e. the flow is inviscid (no air viscosity) and there are no losses at the tips. The disc has the characteristic that it reduces the flow speed and extracts all the energy resulting from the reduction of the flow speed.

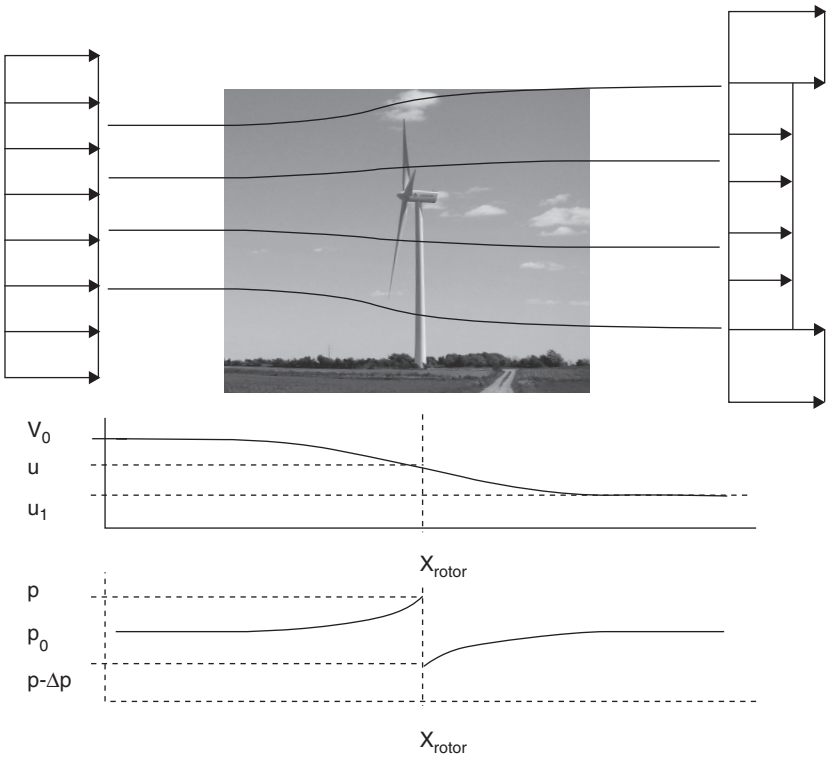

3.2 Sketch of flow around the ideal wind turbine rotor. (*Source*: Photo: Vestas V80 at Tjæreborg Enge, Denmark, by Christian Bak, DTU Wind Energy.).

In Fig. 3.2, a sketch of the flow around an ideal wind turbine rotor is shown, where the development of the velocity and pressure from far upstream of the rotor to far downstream of the rotor is shown.

From Bernoulli's equation, it is possible to make a connection between pressure and velocity both upstream and downstream of the rotor. Bernoulli's equation states that along a stream line the dynamic pressure, determined by the flow speed, added to the static pressure equals the total pressure, Equation [3.1]:

$$\frac{1}{2}\rho u^2 + p = H \qquad [3.1]$$

From the equation, it can be seen that when the velocity decreases, the pressure will increase and vice versa. However, this equation is not valid

through the rotor plane, though the flow upstream and downstream of the rotor plane can be analyzed. Upstream, the connection is as described in Equation [3.2]:

$$p_0 + \frac{1}{2}\rho V_0^2 = p + \frac{1}{2}\rho u^2 \quad [3.2]$$

Downstream of the rotor, the connection is as described in Equation [3.3]:

$$P_0 + \frac{1}{2}\rho u_1^2 = p - \Delta p + \frac{1}{2}\rho u^2 \quad [3.3]$$

By subtracting Equations [3.2] and [3.3] from each other, an expression of the pressure drop through the rotor plane is obtained, Equation [3.4]:

$$\Delta p = \frac{1}{2}\rho(V_0^2 - u_1^2) \quad [3.4]$$

The pressure drop can also be expressed as the change in momentum of the air passing through a unit area of the rotor per second,[8] Equation [3.5]:

$$\Delta p = \rho u(V_0 - u_1) \quad [3.5]$$

Coupling Equations [3.4] and [3.5] gives the following result, Equation [3.6]:

$$u = \frac{1}{2}(V_0 + u_1) \quad [3.6]$$

Equation [3.6] tells us that the air speed in the rotor plane has been decelerated to exactly half of the total velocity deficit that it will experience from far upstream to far downstream in the rotor wake. Thus, the other half of the deceleration of the wind takes place in the wake, downstream of the rotor.

In this context, a convenient entity to be defined is the axial induction factor, a, defined as in Equation [3.7]:

$$u = (1 - a)V_0 \quad [3.7]$$

Therefore, from Equation [3.6] we get $u_1 = (1-2a)V_0$ and the following expression for the extracted power, P, and the corresponding thrust, T, are, Equations [3.8] and [3.9][8]:

$$P = \frac{1}{2}\rho u(V_0^2 - u_1^2)A = 2\rho a(1-a)^2 V_0^3 A \quad [3.8]$$

$$T = \Delta pA = 2\rho a(1-a)V_0^2 A \quad [3.9]$$

The rate of the kinetic energy through the rotor disc, P_{wind}, and the stagnation pressure on the rotor disc, T_{wind}, are, Equations [3.10] and [3.11]:

$$P_{\text{wind}} = \frac{1}{2}\rho V_0^3 A \quad [3.10]$$

$$T_{\text{wind}} = \frac{1}{2}\rho V_0^2 A \quad [3.11]$$

Nondimensional coefficients for the power and the thrust are convenient to use and can be defined using Equations [3.10] and [3.11] as follows, Equations [3.12] and [3.13]:

$$C_P = \frac{P}{P_{\text{wind}}} = \frac{P}{(1/2)\rho V_0^3 A} \quad [3.12]$$

$$C_T = \frac{T}{T_{\text{wind}}} = \frac{T}{(1/2)\rho V_0^2 A} \quad [3.13]$$

Using this definition, Equations [3.8] and [3.9] can be written as Equations [3.14] and [3.15]:

$$C_p = 4a(1-a)^2 \quad [3.14]$$

$$C_T = 4a(1-a) \quad [3.15]$$

Equation [3.14] is very important for understanding wind power extraction, because it tells us that the maximum obtainable power from the wind is $C_P = 16/27$ (approximately 0.593) and that this maximum value is obtained for an axial induction factor of $a = 1/3$. This means that not all of the existing wind power can be extracted but only 0.593 at the very maximum. This maximum limit is usually called the Betz limit.[19] This means that the maximum power is extracted when the wind speed is decreased by 1/3 of the free wind speed in the rotor plane and by 2/3 of the free wind speed in the far wake. An explanation as to why not all power can be extracted is the need to transport the air away from the rotor after the power has been extracted. If the air were completely stopped and all existing power extracted, the air would have to be accumulated somewhere. Thus the remaining power in the wind is required to transport the air downstream and away from the rotor disc. From Equation [3.15] it is seen that the corresponding thrust coefficient, C_T, is 8/9 (approximately 0.89).

As shown in Fig. 3.3, both C_P and C_T are increasing for increasing axial induction a for small values of a. However, for $a > 1/3$, C_P decreases while C_T still increases. For $a > 1/3$, the theory is increasingly uncertain compared to real rotor aerodynamics. For $a = 0.5$, the far wake has reached a standstill and for $a > 0.5$ reversed flow in the far wake is the result. Thus, for $a \geq 0.5$ the theory breaks down. According to the theory $C_T = 1$ for $a = 0.5$ and the rotor is said to be highly loaded. However, in reality the rotor may be even more loaded, because the assumptions used in the derivation of the theory no longer hold for $a > 1/3$. Corrections for $a > 1/3$ will be given in the next section.

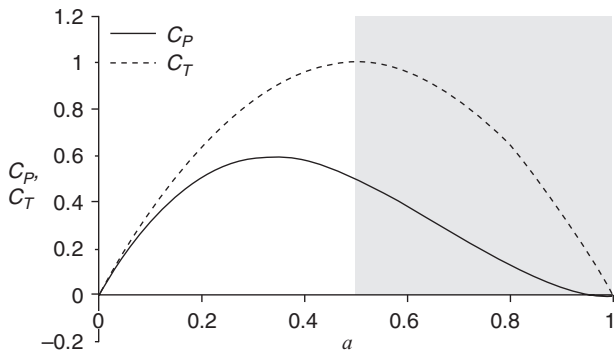

3.3 The power coefficient (C_P) and thrust coefficient (C_T) for one-dimensional momentum theory as a function of axial induction (a).

3.2.2 Blade element momentum theory

Even though the flow through a wind turbine is very complex due to the tip and root vortices and the mutual interaction of the wind flows among the rotor blades, it is possible to simplify the mechanisms in a very efficient way. As shown in Fig. 3.4, the rotor can be divided into annular elements of span width, *dr*. Because the theory that will be developed in this section is based on the one-dimensional momentum theory, it must be assumed that there is no interaction between neighboring elements, something which one-dimensional momentum theory can show to be a good assumption.[8] Also, it must be assumed that the axial and tangential velocity are uniformly distributed all over the annular element. This means that the forces are not concentrated on the blades, but are smeared out over the annular element.

Figure 3.5 shows a section on the rotor blade illustrating the symbols used in the Blade Element Momentum formulation. The blade section is exposed to the axial velocity (wind speed) V_0 and the tangential velocity (eigen

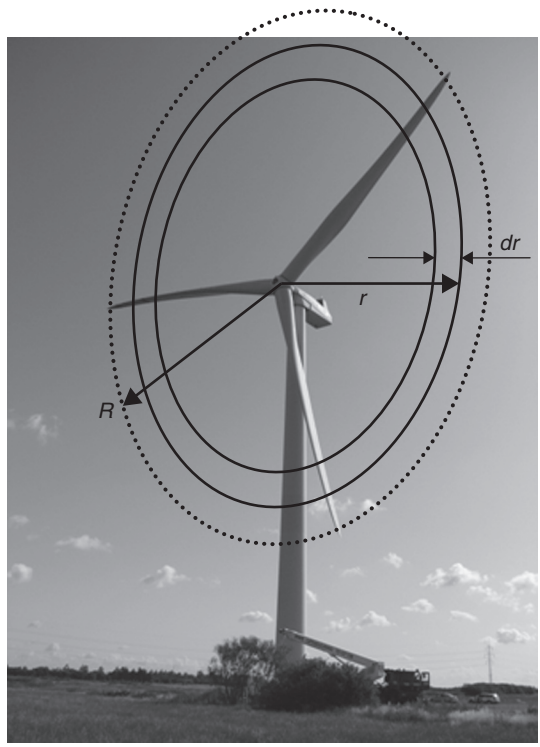

3.4 Sketch of the division of a wind turbine rotor into annular elements. (*Source*: Photo: NM80 at Tjæreborg Enge, Denmark by Christian Bak, DTU Wind Energy.)

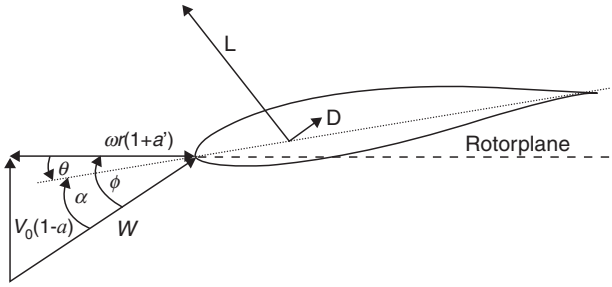

3.5 Sketch of a section on the rotor blade illustrating the symbols used in the Blade Element Momentum formulation. The arrows show the direction of positive values.

velocity) $r\omega$. Because of the forces from the rotor on the wind, where the total induced velocity is parallel to the lift force but in the opposite direction, the axial velocity is reduced to $(1 - a)V_0$, and the tangential velocity is increased to $(1 + a')r\omega$. The resulting velocity that the blade section experiences, the relative velocity, W, is the vector sum of the axial and tangential velocity. The angle from W to the rotor plane is called the inflow angle, ϕ. The blade section is in general twisted, θ, positive in an anticlockwise direction. The twist is defined as the angle from the rotor plane to the airfoil chord line, which is from the very leading edge of the airfoil to the very trailing edge of the airfoil. The angle from the relative velocity, W, to the chord line is called the angle of attack, α.

Based on the sketch in Fig. 3.5, the following relations can be derived, Equations [3.16] and [3.17]:

$$\alpha = \phi - \theta \qquad [3.16]$$

$$\tan\phi = \frac{1-a}{1+a'}\frac{V_0}{r\omega} \Leftrightarrow \phi = \arctan\left(\frac{1-a}{1+a'}\frac{V_0}{r\omega}\right) \qquad [3.17]$$

From the principles of wing section theory, see, e.g. Abbot and Doenhoff,[20] the lift and drag forces per length on each blade section, respectively, can be expressed in terms of respectively lift and drag coefficients as, Equations [3.18] and [3.19]:

$$l = \frac{1}{2}\rho W^2 c c_l \qquad [3.18]$$

$$d = \frac{1}{2}\rho W^2 c c_d \qquad [3.19]$$

Here, c is the chord length and c_l and c_d are the lift and drag coefficients per meter, respectively. These coefficients are described further in Section 3.3.1 and in Chapter 4. For each annular element, the thrust and torque, respectively, are

$$\mathrm{d}T = \frac{1}{2}\rho W^2 c B c_y \mathrm{d}r \qquad [3.20]$$

$$\mathrm{d}Q = \frac{1}{2}\rho W^2 c B c_x r \mathrm{d}r \qquad [3.21]$$

Here, the force coefficients normal to the rotor plane, c_y, and parallel to the rotor plane, c_x, have been used

$$c_y = c_l \cos\phi + c_d \sin\phi \qquad [3.22]$$

and

$$c_x = c_l \sin\phi - c_d \cos\phi. \qquad [3.23]$$

To combine the forces from the blade elements with the results from the momentum theory, the response from the tangential forces must be taken into account. Therefore, the one-dimensional theory, described in the previous section, where the wake rotation is not part of the theory, must be extended with a rotational part reflecting the momentum in tangential direction. Furthermore, a correction for a finite number of blades will be included as shown in Equations [3.24] and [3.25]:

$$\mathrm{d}T = \rho u (V_0 - u_1) F \mathrm{d}A \Leftrightarrow \mathrm{d}T = \frac{1}{2}\rho V_0^2 4Fa(1-a)2\pi r \mathrm{d}r \qquad [3.24]$$

$$\mathrm{d}Q = \rho u u_t r F \mathrm{d}A \Leftrightarrow \mathrm{d}Q = \frac{1}{2}\rho V_0^2 4F(1-a)a' \frac{\omega r}{V_0} r 2\pi r \mathrm{d}r \qquad [3.25]$$

Here u_t is the tangential velocity caused by the wake rotation in the far wake, a' is the tangential induction factor and F is the Prandtl correction for a finite number of blades described by Glauert:[15]

$$F = \frac{2}{\pi}\arccos(e^{-f}) \quad \text{with} \quad f = \frac{B}{2}\frac{R-r}{r\sin\phi} \qquad [3.26]$$

The above formulation of thrust and torque for an annular blade element, Equations [3.20] and [3.21], can now be used in combination with the extended momentum theory, Equations [3.24] and [3.25]. The result can be written as:

$$\frac{a}{1-a} = \frac{1}{4}\frac{1}{F\sin^2\phi}\frac{cB}{2\pi r}c_y \qquad [3.27]$$

$$\frac{a'}{1+a'} = \frac{1}{4}\frac{1}{F\sin\phi\cos\phi}\frac{cB}{2\pi r}c_{x'} \qquad [3.28]$$

With the solidity of the rotor defined as

$$\sigma = \frac{cB}{2\pi r} \qquad [3.29]$$

the axial and tangential induction, respectively, can be written as:

$$a = \frac{1}{\left(4F\sin^2\phi/\sigma c_y\right)+1} \qquad [3.30]$$

$$a' = \frac{1}{\left(4F\sin\phi\cos\phi/\sigma c_x\right)-1} \qquad [3.31]$$

These equations have to be solved iteratively because F, θ, c_y and c_x are all dependent on the induction factors, a and a'. Moreover, the equations are not in agreement with real rotor flow when an axial induction value, a, greater than approximately 1/3 is obtained. The BEM theory assumes no, or small, expansion of the wake. Therefore, the thrust coefficient must be corrected for $a > 1/3$ to be in agreement with real rotor flows. Glauert[15] showed

how such a correction and different empirical relations between the axial induction, a, and the thrust coefficient, C_T, can be made so as to fit measurements, such as the one described by Hansen[18]:

$$C_T = \begin{cases} 4a(1-a)F & a \le 1/3 \\ 4a(1-\frac{1}{4}(5-3a)a)F & a > 1/3 \end{cases} \quad [3.32]$$

Thus, using the above equations, Equations [3.16]–[3.21], [3.26], [3.30]–[3.32], the rotor aerodynamics can be predicted for all wind speeds. However, before doing this, it is necessary to consider important parameters in rotor design and airfoil characteristics, as outlined in the following sections.

3.3 Important parameters in aerodynamic rotor design

The momentum theory described in the previous section provides the basis for the aerodynamic design of wind turbine rotors. As described earlier, the main driver in the wind turbine design is to minimize the cost of energy. This is done by obtaining the correct ratio between capital cost (e.g. cost of materials and rental of workshop) and energy production. However, irrespective of the constraints that operate to reduce the wind turbine cost, it is important to maximize power production while taking account of the constraints.

The power coefficient in an annular element of the rotor disc can be expressed as, Equation [3.33], where $F_{\text{tangential}}$ describes the force per length unit in tangential direction on an airfoil section and in the rotor plane

$$C_p = \frac{r\omega F_{\text{tangential}}\,\mathrm{d}r}{(1/2)\rho V_0^3\,\mathrm{d}A} \Leftrightarrow$$

$$C_P = \frac{r\omega \tfrac{1}{2}\rho(((1-a)V_0)^2 + ((1+a')r\omega)^2)c_x cB\,\mathrm{d}r}{\tfrac{1}{2}\rho V_0^3 2\pi r\,\mathrm{d}r} \Leftrightarrow$$

$$C_P = \frac{(((1-a)V_0)^2 + ((1+a')r\omega)^2)}{V_0^2}\frac{r\omega}{V_0}\frac{cB}{2\pi r}c_x \quad [3.33]$$

Defining

$$\lambda = \frac{\omega R}{V_0} \quad [3.34]$$

as the tip speed ratio between the eigen speed of the blade tip and the free wind speed and

$$\lambda_{\text{loc}} = \lambda \frac{r}{R} \qquad [3.35]$$

as the local speed ratio between the eigen speed of the blade at a certain radius and the free wind speed, and using Equation [3.29], results in the following expression for the power coefficient, Equation [3.36]:

$$C_P = \left((1-a)^2 + \left(\lambda \frac{r}{R} \right)^2 (1+a')^2 \right) \lambda \frac{r}{R} \sigma c_x = f\left(\lambda \frac{r}{R}, \sigma c_x, a, a' \right) \qquad [3.36]$$

This equation is important in aerodynamic blade design because it tells us that the power coefficient at a certain rotor radius is dependent on the tip speed ratio, λ, the position relative to the tip, r/R, the solidity of the rotor, σ, the force coefficient in the rotor plane, c_x, and induction factors in axial and tangential direction, a and a', respectively. Deriving the thrust coefficient the same way results in the following expression, Equation [3.37]:

$$C_T = \left((1-a)^2 + \left(\lambda \frac{r}{R} \right)^2 (1+a')^2 \right) \sigma c_y = f\left(\lambda \frac{r}{R}, \sigma c_y, a, a' \right) \qquad [3.37]$$

Even though this relation for the thrust coefficient is somewhat different from the relation for the power coefficient, it tells us that the thrust coefficient is dependent on the same parameters as the power coefficient except that the force coefficient normal to the rotor plane, c_y, and not in the rotor plane, c_x, contributes to the thrust. Because the forces and the induction factors are unambiguously connected, and σ and c_x (and c_y) are always used together as in, e.g. Equations [3.30], [3.31], [3.36] and [3.37], C_P and C_T in an annular element can briefly be described by the functions $f(\lambda r/R, \sigma c_x)$ and $f(\lambda r/R, \sigma c_y)$, respectively, meaning that only two parameters in each function control the rotor design. Since c_x and c_y are strongly correlated to c_l (see Equations [3.23] and [3.22], respectively), the rotor design can with very good approximation be described by the function $f(\lambda r/R, \sigma c_l)$. Thus, keeping the local speed ratio, $\lambda r/R$, constant, the term σc_l needs to be kept constant to maintain power production. Therefore, if a blade designer wants to design slender blades the solidity, σ, needs to be reduced, but the lift coefficient, c_l, then needs to be increased to keep σc_l constant. If the designers wants wider blades, σ needs to be increased, but then c_l needs to be decreased.

The following shows how the blade chord can be computed if the rotor is designed for maximum power. Based on Equation [3.14], it follows that maximum C_P is ideally 16/27 and that this value is obtained for $a = 1/3$. Using Equation [3.29], and isolating σ while putting $a = 1/3$ in Equation [3.30], gives the following expression, Equation [3.38]:

$$\frac{2\sin^2\phi F}{c_y} = \frac{Bc}{2\pi r}$$

$$c = 4\pi r \sin^2\phi F \frac{1}{c_y}\frac{1}{B}$$

$$\frac{c}{R} = 4\pi\frac{r}{R}\sin^2\left(\arctan\left(\frac{(2/3)}{(1+a')}\frac{1}{\lambda}\frac{1}{r/R}\right)\right)F\frac{1}{c_y}\frac{1}{B} = f(a', \lambda\frac{r}{R}, F, c_y, B) \quad [3.38]$$

Here, Equations [3.17] and [3.35] are also used for expressing the chord of the blade using the same parameters as in Equations [3.36] and [3.37]. Thus, as stated in Equation [3.38], the normalized chord, c/R, is dependent on the normalized radius, r/R, the tangential induction factor, a' (the axial induction factor, a, is locked to 1/3), the tip speed ratio, λ, the correction for number of blades, F, the force coefficient normal to the rotor disc, c_y, and the number of blades, B.

The equations need to be solved iteratively and some results are shown in Fig. 3.6, assuming that the chosen c_l (closely correlated to c_y) and α is constant for the whole blade. Apart from Equations [3.16] and [3.38], Equation [3.31] must also be solved. Note that increasing c_l (and thereby c_y), B and λ (also called tip speed ratio, TSR) leads to a reduction in the chord distribution.

In addition to predicting the aerodynamic design, the twist angle of the blade must also be calculated. This can be derived from Equation [3.16],

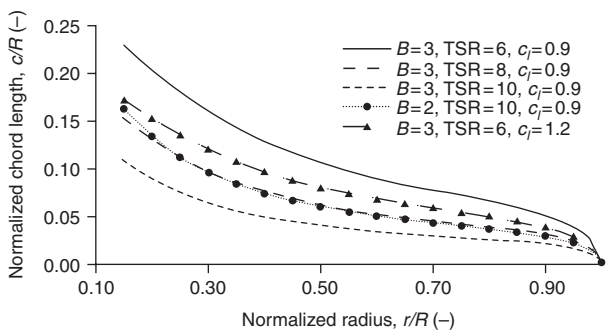

3.6 Example of the chord distribution with different number of blades, different force coefficients normal to the rotor plane and different tip speed ratios, TSRs.

which shows the relation between the inflow angle, the angle of attack and the twist. The inflow angle is known when predicting the induction factor, a', and the angle of attack is determined from the airfoil characteristics: good airfoil performance, in combination with robust operation, is a factor to be considered when the angle of attack is chosen.

Even though it is very important to design a rotor with high efficiency, it can sometimes be an advantage to decrease the load slightly to save costs on other components in the wind turbine, e.g. the tower. Loads can be reduced by operating the rotor at a lower rotational speed than it has been designed for, but the rotor can also be designed to have an axial induction lower than $a = 1/3$. To do so, Equation [3.38] can be generalized as shown in Equation [3.39].

$$c = 4\pi r \sin^2\phi F \frac{1}{c_y}\frac{1}{B}\frac{2a}{(1-a)}$$

$$\frac{c}{R} = 4\pi\frac{r}{R}\sin^2\left(\arctan\left(\frac{1-a}{(1+a')}\frac{1}{\lambda}\frac{1}{r/R}\right)\right)F\frac{1}{c_y}\frac{1}{B}\frac{2a}{(1-a)} = f(a,a',\lambda\frac{r}{R},F,c_y,B) \quad [3.39]$$

3.3.1 Airfoil performance

As seen in the previous section, important parameters in aerodynamic blade design are the force coefficients in the rotor plane, c_x, and out of the rotor plane, c_y. It is seen from Equations [3.22] and [3.23] that these coefficients are derived from the coefficients c_l and c_d, the lift and drag coefficients, respectively. In Fig. 3.5 the directions of lift and drag are shown. The lift is always normal to the incoming flow whereas the drag is always in the direction of the flow. Thus, the angle of attack, α, gives these directions relative to the airfoil chord. In Fig. 3.7 a sketch of the airfoil characteristics is seen.

To the right is seen the lift coefficient, c_l, vs angle of attack, α, and to the left is seen c_l vs the drag coefficient, c_d, where the coefficients are normalized according to Equations [3.18] and [3.19]. For low α and low c_l, c_d is rather constant and corresponds to a flow around the airfoil which is mainly attached to the surface. For higher α and c_l and approaching maximum c_l, c_d is increasing, which reflects the start of separation typically from the trailing edge. Increasing α will increase the amount of separation, which at the end will cause the airfoil to stall from the leading edge with massively separated flow. Because c_l can be interpreted as a production term and c_d as a loss term, a measure for the airfoil efficiency is the lift–drag ratio, c_l/c_d. The fine dashed line in the left plot illustrates this. The steeper the slope of this line

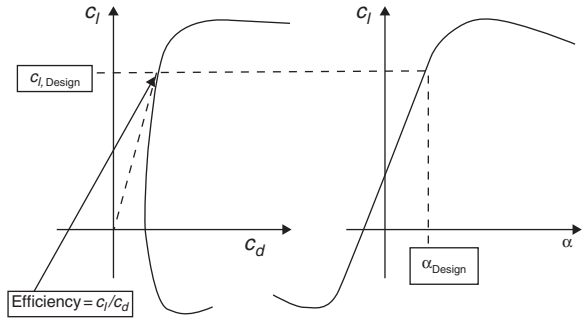

3.7 Sketch of the airfoil characteristics measured by c_l, c_d and α.

starting in origin, the more efficient the airfoil is. According to Equations [3.22] and [3.23], the normal and tangential force coefficients can be written as, Equations [3.40] and [3.41]:

$$c_x = c_l \sin\phi - c_d \cos\phi \Leftrightarrow c_x = c_l\left(\sin\phi - \frac{1}{c_l / c_d}\cos\phi\right) \quad [3.40]$$

$$c_y = c_l \cos\phi + c_d \sin\phi \Leftrightarrow c_y = c_l\left(\cos\phi + \frac{1}{c_l / c_d}\sin\phi\right) \quad [3.41]$$

Equations [3.40] and [3.41] reflect that the in-plane force coefficient contributing to the power is dependent on the lift coefficient, c_l, the inverse lift–drag ratio, c_l/c_d and the inflow angle ϕ. Thus, an airfoil for use on a wind turbine should operate at a point with high c_l/c_d. Commonly, the point at which we find maximum c_l/c_d is called the design point, with the corresponding design lift, $c_{l,\text{design}}$, and design angle of attack, α_{design}. How the c_l/c_d influences the performance of a rotor is shown in Fig. 3.8.

The figure shows the viscous loss in the local power coefficient on a rotor in percent as a function of the local speed ratio and how the loss in the local power coefficient depends on c_l/c_d, where the blade element momentum theory has been used in the analysis assuming that the axial induction factor is $a = 1/3$ and that there is no tip loss. The viscous loss in the local power coefficient is defined as, Equation [3.42]:

$$\text{Power} - \text{loss}_{\text{local,viscous}} = \frac{C_{P,\text{local,inviscid}} - C_{P,\text{local.viscous}}}{C_{P,\text{local,inviscid}}} \quad [3.42]$$

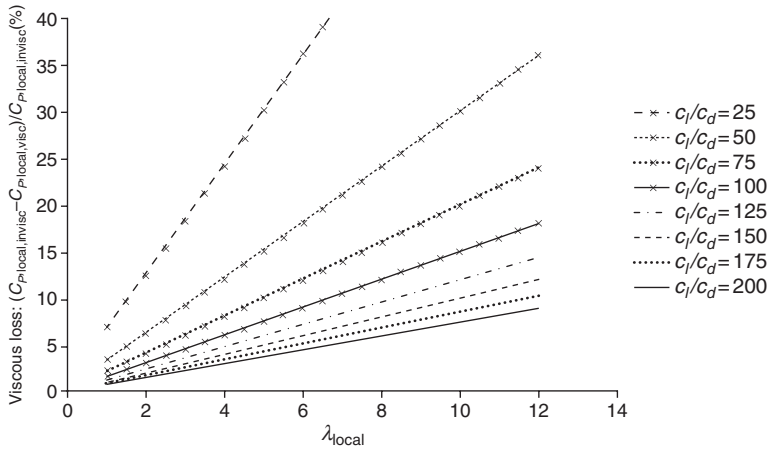

3.8 Local power loss as a function of the local speed ratio for different lift–drag ratios.

where C_P (both $C_{P,\text{local,inviscid}}$ and $C_{P,\text{local,viscous}}$) is computed from Equation [3.36]. In the case of inviscid flow, $c_l/c_d \to \infty$ and in the case of viscous flow c_l/c_d is a finite number. For a common value of c_l/c_d of 100 and for a rotor with a common tip speed ratio of $\lambda = 8$, it can be seen from Fig. 3.8 that such a rotor has at the tip a viscous loss in the local power coefficient of approximately 12% ($\lambda_{\text{loc}} = 8$), but at 25% radius (corresponding to $\lambda_{\text{loc}} = 2$) the viscous loss is only 3%. In relation to this it is important to note that for a rotor, λ_{loc} is proportional to the radius as stated in Equation [3.35]. To analyze Fig. 3.8 further, in addition to the above assumptions ($a = 1/3$ and no tip loss), it can be assumed that the tangential induction is small, $a' << 1$, which is a good approximation except at very low values of $\lambda_{\text{loc}} < 1$. With these assumptions Equation [3.42] reduces to a very simple expression, Equation [3.43]:

$$\text{Power} - \text{loss}_{\text{local,viscous,simplified}} = \frac{3}{2}\frac{\lambda_{\text{loc}}}{c_l / c_d} \qquad [3.43]$$

Equation [3.43] shows that the viscous loss in the local power coefficient increases directly proportional to λ_{loc} and inversely proportional to c_l/c_d. The variation in viscous losses, depending on $\lambda_{\text{loc,}}$ illustrates that it is more important to increase c_l/c_d on the outer part of the rotor than on the inner part. This conclusion is very important, because the viscous loss in the local power coefficient should be weighted with the corresponding area of the annular element of the rotor to predict the absolute viscous power loss in

the annular element measured in Watts. Thus, the absolute viscous power loss in an annular element is proportional to $r \times \text{Power} - \text{loss}_{\text{viscous}}$. According to Equations [3.43] and [3.35] this is proportional to $r^2 \lambda / R(c_l / c_d))$, which means that a high c_l/c_d on the outer part of rotors is even more important. The above considerations are important in the choice of airfoils, but can also be used in the choice of the design tip speed ratio. However, some considerations about the design tip speed ratio are described in Section 3.5.7.

In addition to focusing on the c_l/c_d when selecting airfoils, it is important also to focus on the lift coefficient according to Equation [3.40]. If airfoils are selected to create maximum power it is important that they can generate sufficient lift to obtain maximum power, i.e. to obtain an induction of $a = 1/3$ according to the blade element momentum method. This is also the case for thick airfoils that commonly are mounted on the inner parts of rotors even though they often show rather low lift coefficients. However, it should be emphasized that rotors should be designed to achieve a trade off between power and loads in order to minimize the cost of energy and thus the entire rotor should not necessarily show maximum local power coefficients at all radial positions.

Since c_l and c_l/c_d are created by the airfoil in the flow field, it is important to be aware that the airfoil characteristics, c_l and c_d, as sketched in Fig. 3.7 are not a fixed set of data, but depend on several parameters. Among these the most important parameters that influence the aerodynamic performance are:

- the Reynolds number,
- the relative thickness of the airfoil,
- the airfoil shape, and
- whether the airfoil surface is clean or contaminated.

Further information about airfoil performance is described in Chapter 4.

3.4 Particular design parameters

The design of blades requires more than aerodynamic models and knowledge of airfoil performance. The choice of the generator, the tip speed and other constraints need to be selected. In this section these subjects will be addressed.

3.4.1 Tip speed ratio

As seen in Section 3.3 the tip speed ratio, λ, is an important parameter when designing a rotor. When analyzing the influence of λ on the power

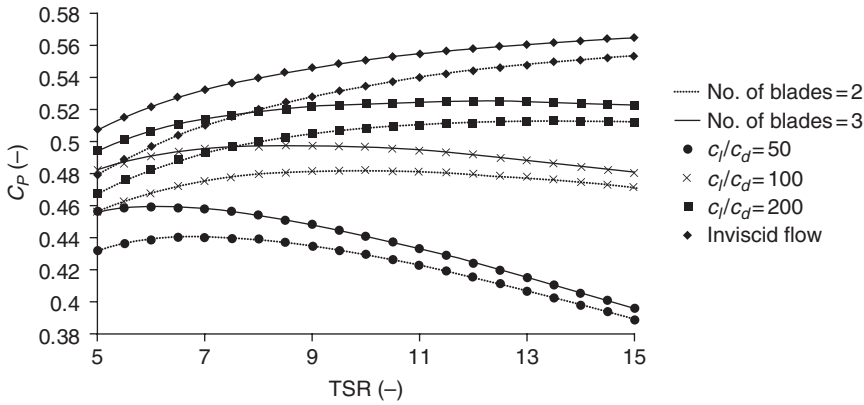

3.9 Power coefficient C_P vs tip speed ratio (TSR), λ.

performance, it turns out that λ should be increased to reduce the tip loss. For ideal rotors in inviscid flow, λ should be increased as much as possible, and in theory to infinity, if the target is to maximize power production. However, for real viscous flows the lift–drag ratio of the airfoils counteracts this and λ is limited to between 5 and 12 for rotors between 1 kW and 5 MW depending on the lift–drag ratio and the number of blades.[21] Figure 3.9 shows the relation between the power coefficient, C_P, and λ assuming that the lift–drag ratio is constant for the entire blade. Thus, knowing the approximate lift–drag ratio of the airfoils used on the blades (Fig. 3.9) indicates which λ to choose with respect to C_P. However, aspects other than power production can be important such as the need to reduce the load, considerations concerning the blade structure, generator torque (which can be reduced by increasing the rotational speed) and noise caused by high tip speed.

3.4.2 Size of rotor/generator

As described above, the design of a rotor is an integral part of the design process for the wind turbine as a whole. The overall goal is to manufacture a wind turbine at lowest cost per energy unit. Therefore, the target when designing a wind turbine rotor is not necessarily to capture the maximum energy at a certain site or the maximum power at a certain (typical) wind speed, but rather to capture as much energy as possible while keeping the cost of all components, from generator and tower to foundation and grid connection, as low as possible.

The size of the rotor is of primary importance when considering the total cost of the wind turbine. With a bigger rotor, more energy can be captured; however this is likely to mean higher loads and a larger generator. At the

very least it is important to determine the 'rated power', which is the maximum of the mean power output averaged in a period of 10 min. In general, the rated power correlates with the maximum loads in the normal operation of the wind turbine. The 'rated wind speed' is the wind speed at which the rated power is obtained. This wind speed depends on the rotor size, which again depends on the wind climate at a certain site. Therefore a decision on where the wind turbine is likely to be erected is needed. In traditional rotor designs, the rated wind speed is often deemed to be the mean wind speed at a site plus approximately 6 m/s. Thus, if the mean wind speed is 8 m/s, the rated wind speed will be around 14 m/s. This, however, is a rule of thumb, and therefore the choice of rotor size should be based on the specific wind climate, corresponding loads and cost estimations. Recently especially, there has been a trend towards decreasing the range between mean wind speed and rated wind speed, resulting in designs with rather big rotors when compared to the generator size.

A simple way to produce a rough estimate of the rotor size is to decide on the rated power and rated wind speed and use the following procedure. Based on analysis of existing rotor designs, the mechanical power coefficient (which is the efficiency without the loss in generator and gearbox), $C_{P,\text{rated}}$ (see Equation [3.13]), is often between 0.25 and 0.30 at rated wind speed. The radius of the rotor will then be, Equation [3.44]:

$$R = \sqrt{\frac{P_{\text{rated}}}{(1/2)\rho V_{\text{rated}}^3 C_{P,\text{rated}} \pi}} \qquad [3.44]$$

Here the rotor area or the area through which the blades sweep, known as the swept area, A, from Equation [3.12] is $A = \pi r^2$. Choosing P_{rated} to 1 MW and V_{rated} = 14 m/s, which corresponds to a site with medium to high wind speed, and assuming air density at standard conditions, ρ = 1.225 kg/m^3, we get R = 27.5 m and a rotor diameter of 55.0 m if $C_{P,\text{rated}}$ is chosen to 0.25.

3.4.3 Rotor control

As shown in Sections 3.3 and 3.5.7, the rotor design is dependent, among other parameters, on the tip speed ratio. Therefore, a certain tip speed ratio, λ, must be chosen. To operate the rotor so as to extract maximum power, the ratio between the tip speed and the wind speed must be constant. This means that for increasing wind speed, the tip speed should be increased correspondingly if this is possible according to the choice of generator. However, because of, e.g. noise and erosion of the leading edge, the tip speed should not increase too much. For large modern wind turbines, maximum tip speeds

of 70–90 m/s are common. Therefore, for several reasons it is desirable to limit the tip speed and thereby the rotational speed. Which maximum rotational speed to choose should also depend on an analysis of the total wind turbine cost as described in Section 3.4.2.

As well as λ, the type of rotor control to be used to limit the turbine's power needs to be chosen. The size of the generator and the allowable loads on the turbine determines at which level output should be limited. This limitation is carried out by increasing the drag or decreasing the lift on the airfoil sections. In modern wind turbines this can be done actively by pitching the blades, to decrease the lift on the outboard part of the blade, or passively by letting the blades stall, to increase the drag.

It is now accepted that making an aerodynamic design of a wind turbine rotor requires knowledge of the methods and principles of rotor control, so that such things as whether the turbine should operate with or without stalled condition, and whether the airfoils have the required reserve from design lift to maximum lift, can be known. Several different types of rotor control are possible, the most common of which are described below.

- **Constant/variable rotational rotor speed.** This degree of freedom in the control depends on the characteristics of the generator. If a constant rotor speed is chosen, a simpler and less costly generator can be chosen. However, choosing a variable speed rotor makes it possible to optimize the power for a large range of wind speeds. Also, using this kind of generator creates more flexibility in the connection to the power grid.
- **Pitchable/fixed blades.** Pitchable blades allow the freedom to limit and optimize the power very precisely and also make it possible to stop the turbine, e.g. in emergency situations. When limiting the power, the pitchable blades can be used to reduce the lift or increase the drag by either decreasing or increasing the angle of attack, respectively. Decreasing the angle of attack ensures that the flow is attached to the airfoils so that the operation of the airfoils will be in the linear part of the lift curve; this is called 'pitch control'. Increasing the angle of attack to stall/deep stall ensures a nearly passive limitation of the power because only minor changes to the pitch setting are generally needed; this is called 'active stall control'.
- **Pitch/stall control.** Turbines limit the power by reducing the lift coefficient or increasing the drag coefficient for increasing wind speeds, either in the linear part of the lift curve by reducing the angle of attack (pitch control), or in the stall part of the lift curve by increasing the angle of attack (stall control), respectively. Using fixed blades and constant rotational rotor speed, one is forced to use stall control. This is illustrated in Fig. 3.10, where the power curve is shown to the left with the corresponding airfoil operation in terms of a lift curve to the right.

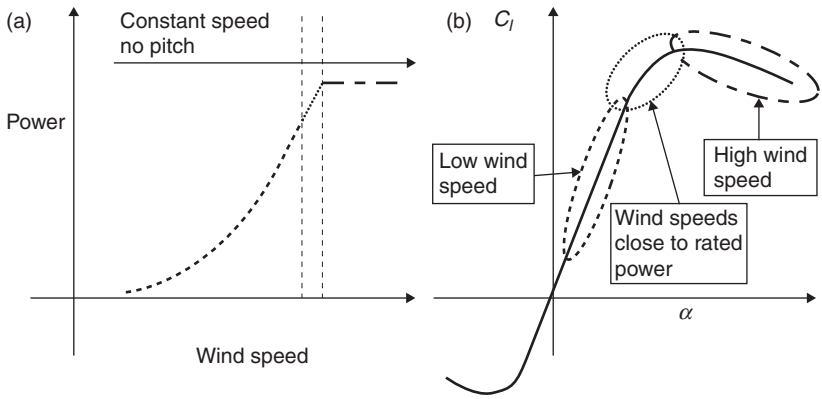

3.10 Sketch of the principle behind Stall Regulation shown on the power curve (power vs wind speed), (a), and the lift curve (lift coefficient vs angle of attack), (b).

At low wind speeds the angle of attack is low and the lift is thereby also low (dashed lines), operating around maximum lift–drag ratio. The dotted line shows operation at wind speeds close to rated power and at corresponding lift values close to and at maximum lift. The dot-and-dash line shows the operation at high wind speeds where rated power is obtained, and the corresponding operation at high angles of attack in stall, resulting in a (nearly) passive limitation of the power. The stall regulation was a common concept for wind turbines of up to around 2 MW.

Using pitchable blades, both pitch and stall control are possible. However, the (active) stall controlled rotors have, in the case of the bigger rotors of between 500 kW and 2 MW, sometimes exhibited negative aerodynamic damping, which causes undesirable vibrations. Also, the (active) stall controlled rotors experience relatively high loads at high wind speeds compared to the pitch controlled rotors. Using pitch control requires much higher pitch activity, but because stall is avoided, the flow is more reliable and predictable. The pitch control concept is illustrated in Fig. 3.11, where, additionally, variable rotor speed is used at low wind speeds. This kind of control is pitch control in combination with variable rotor speed and is called pitch regulation variable speed (PRVS). Apart from variable rotor speed at low wind speeds, which is used to obtain constant tip speed ratio (λ or *TSR*), the blades will be pitched to limit output at high wind speeds. However, the blades can in some cases also be pitched for wind speeds between the region of variable rotor speed and the region with power limitation. In Fig. 3.11, it

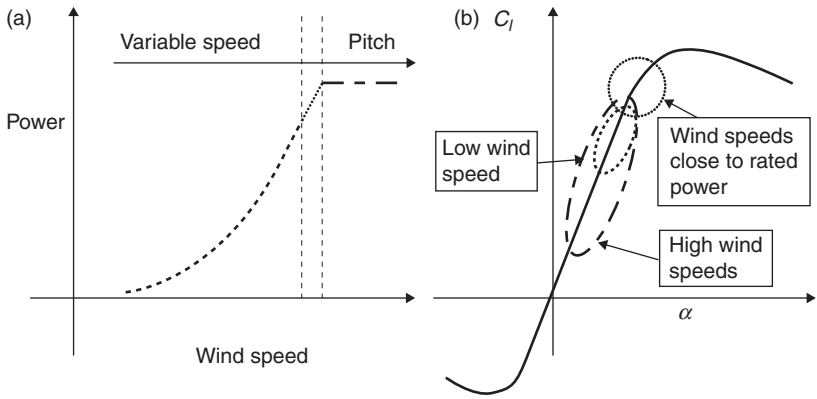

3.11 Sketch of the principle behind pitch regulated variable speed (PRVS) showed on (a) the power curve (power vs wind speed) and (b) the lift curve (lift coefficient vs angle of attack).

can be seen that the angle of attack is low at high wind (dotted-and-dashed lines) and high (but not entering stall) close to rated power (dotted lines). Furthermore, the rotor load decreases at high wind speeds. Therefore, the loads for a pitch controlled wind turbine will in general be less than for a(n) (active) stall controlled wind turbine. In Fig. 3.11 the dashed line shows operation at low wind speeds at the power curve where the rotor operates at constant tip speed ratio, and corresponding operation at a lift value with high lift–drag ratio.

The common way of controlling today's Mega Watt (MW) turbines is through use of PRVS. However, in the 1970s, 1980s and 1990s, when the rated power of most turbines was below 2 MW, the turbines did not operate as a significant part of the power grid and there were fewer requirements as power quality. Also, the structural dynamics were less sensitive to the aerodynamic damping of the blades. Therefore, a very common control method was stall regulation, with constant rotational speed combined with fixed blades.

Thus, the correct choice of rotor control is necessary in order to:

- select airfoils that have proper design lift, maximum lift and stall characteristics;
- design the rotor in such a way that it can start up at a fairly low wind speed;
- design the rotor in such a way that rated power can be kept fairly constant in all high wind speeds;
- design the rotor at the correct tip speed ratio.

3.4.4 Design constraints

Previous sections have pointed out that rotor design should not focus only on maximizing power production, but also on other aspects relevant to the main objective of reducing the cost of energy. Many constraints affect the ability to achieve this ideal, and these are dependent on, e.g. the rotor size and the selected materials. Examples of such constraints are:

- The maximum chord has to be lower than a certain value so that the blade can be transported, e.g. by truck on roads and below bridges. This is not necessarily an issue, however, if the rotor is going to be installed offshore and therefore transported by ship.
- The maximum chord should be such that the extreme loads, e.g. at stand-still, do not cause high loads on other components, such as the tower.
- For structural reasons, the inner part of the blade has to be designed with thicker airfoils than on the outer part of the blade in order to withstand the loads.
- The rotor should be able to cut-in at a fairly low wind speed.
- In order to reduce noise emission the outer part of the blade can be twisted towards lower lift coefficients; this is because, according to current knowledge, noise emission increases for increasing angle of attack.[22]
- The rotor speed has to be limited to prevent excessive loads on the whole wind turbine. However, for a given power, the loads on the shaft and the generator reduce with increasing rotor speed. Therefore the maximum rotor speed should be selected appropriately.
- As illustrated in Fig. 3.3, the thrust coefficient, which in general relates to the loads on many component parts of the wind turbine, can be reduced somewhat by reducing a slightly below $a = 1/3$ with only a small reduction in C_P. In this way, loads on the turbine can be reduced significantly without losing too much energy production.
- Pre-bend and/or pre-twist of the blade are options that allow blades to increase their clearance from the tower and obtain the desired twist irrespective of the torsional deformation, respectively. However, these options do not affect the aerodynamic design because the pre-bend ensures the intended maximum rotor area and the pre-twist ensures the intended twist distribution.

There are many other design constraints, depending on the manufacturing process, the particular rotor control concept and the particular wind turbine concept, and so the above is not an exhaustive list of issues, but only indi-

cates some of the most important aspects to be considered as part of the rotor design process.

3.4.5 Choice of number of blades

When choosing the number of blades, several considerations have to be taken into account, such as esthetics, tip loss, structural constraints and Reynolds numbers. Even though the rotor designer will often find that the number of blades is decided by other decision makers, there follows a summary of the relevant design considerations in order to draw a complete picture of the rotor design process.

- **Esthetics.** The design of the complete turbine, including the shape of the nacelle, the spinner and the tower, is important. Likewise the visual impact of the rotating blades is important. These issues pose the question: do two, three or four rotating blades (or even more) look nice?
- **Tip loss.** The rotor becomes more aerodynamically efficient when the number of blades is increased. This is because the distance between the vortex sheets in the wake of the rotor becomes smaller for an increasing number of blades, and therefore flow outside the wake does not flow in between the vortex sheets creating a more diffuse wake and thereby introducing loss. The loss of power efficiency when the number of blades is reduced from three to two is illustrated in Fig. 3.9.
- **Structural considerations.** Increasing the number of blades, for fixed design lift along the blade, reduces the chord length of each blade so as to keep the solidity of the rotor constant. With decreasing chord length, the relative thickness may need to be either increased or maintained, requiring more material to be used in the rotor. The increasing relative thickness generally makes the blade less aerodynamically efficient and the increased amount of material makes it heavier.
- **Reynolds number.** The Reynolds number is proportional to the chord length of the blade and the rotational speed. Therefore, an increase in the number of blades with fixed solidity of the rotor, σ, will result in a decrease of the chord length and thereby a decrease of the Reynolds number. Thus, in terms of Reynolds number, it is desirable to minimize the number of blades.
- **Transportation of blades.** Increasing the number of blades increases the need for transportation. For this reason, too, it is desirable to minimize the number of blades.
- **Manufacturing costs.** Increasing the number of blades increases the need for manpower and space in the manufacturing facility. Thus, reducing the number of blades saves on the costs of rotor manufacture.

3.4.6 Evaluation of the rotor design

When a rotor is aerodynamically designed, it needs to be evaluated to assess the response in terms of power and loads. For this purpose, aerodynamic or aeroelastic codes should be used. Several aerodynamic codes exist, but if an aerodynamic or aeroelastic code is not available, the background for creating an aerodynamic code can be found in Reference 18. Commonly used aeroelastic codes in the wind turbine industry in 2013 are, e.g. FLEX,[23] Bladed,[24] Phatas,[25] FAST[26] and HAWC2.[27] Running full aeroelastic computations also requires knowledge of the structural characteristics of the blades and the entire wind turbine.

An aerodynamic code requires the blade planform in terms of chord and twist as function of radius, rotational speed and pitch as function of wind speed, airfoil characteristics in terms of c_l, c_d and c_m as function of α for the different relative thicknesses along the blade, and possibly also losses in the drive train (gear box and generator) in order to predict the electrical power. This information should be provided as a part of the aerodynamic rotor design process.

3.5 An example of the rotor design process

In this section, a rotor for a 1 MW pitch regulated variable speed (PRVS) wind turbine will be aerodynamically designed. The design process has been simplified so that the power is maximized with no considerations of load reduction, even though it is very important to reduce loads on all the components on the turbine. Thus, the rotor is designed for an axial induction of $a = 1/3$ even though a slightly lower value might be more appropriate for load reduction. The process is divided into steps, but in reality each step can appear more than once because it is an iterative process, with knowledge gained there from sometimes proving to have been relevant for an earlier step. The process described for designing the blade does not require any tools other than a spread sheet or access to a programming language, such as Matlab, FORTRAN or C. However, in the evaluation process an aerodynamic or aeroelastic computer code would greatly facilitate a detailed evaluation of the rotor and the wind turbine. The resulting rotor is not meant as an example of an optimal rotor, but should be viewed only as an illustration of the method.

It should be noted that several steps in the design process are probably irrelevant for many rotor designers, as many parameters will have been specified by other decisions makers. The specified parameters could be for example, wind climate, rotor diameter, rated power and hub height and within these constraints the optimum rotor should be designed. However, for the sake of completeness all steps in the design process are considered.

3.5.1 Step 1: Wind climate

Even though the wind turbine under consideration here could be erected at many different sites, a representative wind climate needs to be agreed upon. Standards exist,[28] in which turbines are classified by site characteristics such as low/high wind speeds and low/high turbulence. However, in this example, for demonstration purposes, it has been decided to erect the turbine on an inland site at Værløse in Denmark, as listed in Reference 29, p. 146, where the Weibull distribution in 10 m height is given as:

$$F\left\{V_{10\,\mathrm{min}} \le V\right\} = 1 - \exp(-(V/A)^k)$$

with $A_{h,\mathrm{measured}} = 4.7$ m/s, $k_{h,\mathrm{measured}} = 1.55$ and $h_{\mathrm{measured}} = 10$ m. The roughness length in Værløse is estimated to $z_0 = 0.01$ m, which corresponds to airport runway areas and terrain surface characteristics ranging from very smooth surfaces, e.g. water areas to smooth surfaces, e.g. farmland. The hub height of the wind turbine is set to 60 m and therefore Weibull parameters for this height should be predicted. However, this hub height is based on a rule of thumb which states that the hub height is approximately equal to the rotor diameter. The rotor diameter is set at approximately 60 m, based on experience of other 1 MW turbine projects. It should be emphasized, however, that the hub height is a decision that is part of the overall design of the wind turbine and depends, among other parameters, on the wind climate, because the increase in wind speed as a function of height varies from site to site. Assuming that the wind shear is logarithmic and there are no changes in roughness close to the site, the wind climate parameters will be:

$$A_h = A_{h,\mathrm{measured}} \frac{\ln(h/z_0)}{\ln(h_{\mathrm{measured}}/z_0)} = 5.9 \text{ m/s}$$

$$k_h = k_{h,\mathrm{measured}} = 1.55$$

3.5.2 Step 2: Size of rotor/generator

The choice of the size of the rotor and generator should be made so that the cost of energy is minimized. In other words, the ratio between the wind turbine cost and the predicted energy production in the lifetime of the wind turbine should be minimized. Therefore, a thorough study should be carried out based either on experience of wind turbine costs or based on cost

models. However, in this case the problem is simplified and, based on the knowledge of factor A_h, which is fairly low, it is decided to choose 12 m/s as the rated wind speed, which is approximately 6 m/s higher than the average wind speed on the site. Maximum C_P at rated wind speed is set to C_P = 0.25, which will be used to estimate the rotor diameter. The rotor size can be predicted using Equation [3.44]. With P_{rated} = 1.0 MW, V_{rated} = 12 m/s, ρ = 1.225 kg/m^3 and C_P = 0.25 the rotor must be designed with a diameter of approximately 70 m or a radius of 35.0 m. It should be noted that the trend in recent years has been towards rather big rotors, when compared to the generator size, so some manufacturers might choose an even bigger rotor diameter and therefore a lower rated wind speed.

3.5.3 Step 3: Rotor control

Even though it has been decided that the rotor control in this case is to be of the pitch regulated variable rotor speed (PRVS) type, it is important at this stage to consider the process for choosing the type of control, as set out in Section 3.4.3. The choice of rotor control will be dependent on the size of the rotor and the wind turbine and on the philosophy of the design. In addition, the components forming part of the rotor control, such as the pitch bearings and the variable speed generator, should be considered in order to take the total cost of the turbine, including operation and maintenance costs, into account.

If it were decided to design a stall controlled rotor the same procedure as sketched in the following Steps 4 to 8 could be used. However, if such a rotor were to operate with constant rotational speed, this speed should be selected and considered in relation to the wind speeds which supply the majority of the annual energy. In addition, account should be taken of the fact that the blade design can result in an excess of power at high winds so that the predicted power from the rotor exceeds the desired rated power. The power at high wind can be reduced by maintaining the twist at the outboard part of the blade and twisting the inner part of the blade so that it enters stall at lower wind speeds.

3.5.4 Step 4: Design constraints

There are a number of constraints which the rotor design should fulfill:

- The maximum chord should be limited. In this case it is set to 3.0 m for transportation reason. However, this limit depends on the capacity of the blade manufacturer to transport the blade.
- The maximum tip speed is set to 75 m/s. This is to reduce the maximum noise emission. The tip speed of 75 m/s corresponds to a maximum rotational speed of 20.46 RPM.

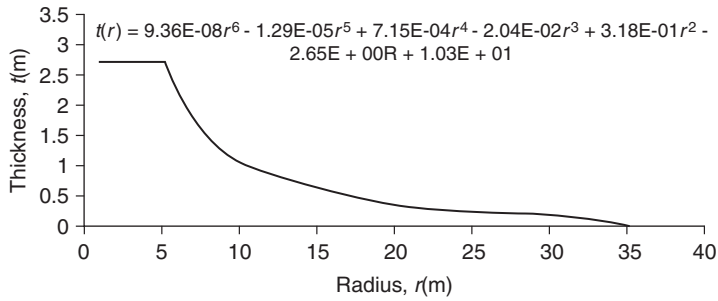

3.12 Initial estimate of the thickness distribution of the blade.

- The initial guess for the thickness of the blade is based on structural considerations. Often the aerodynamic rotor design will be based on a distribution based on experience from an earlier design. The structural design should fulfill different requirements, such as a maximum tip deflection and minimizing the weight (i.e. increasing the thickness) without losing too much aerodynamic efficiency. An example of such a thickness distribution is shown in Fig. 3.12. In this example the thickness distribution should simply be considered as an input to the aerodynamic design process. However, when evaluating the rotor design after the aerodynamic rotor design process is carried out, the weighting between the structural and the aerodynamic performance could possibly change the thickness distribution. In Fig. 3.12, a polynomium is shown to describe the thickness distribution from 5.14 m and outwards. For radii less than 5.14 m, the thickness is constantly 2.70 m.

3.5.5 Step 5: Choice of number of blades

For this size of turbine, the number of blades significantly influences transportation, maintenance and rotor costs. Therefore, the number of blades should be reduced as far as possible without compromising the energy production, loads, noise emission and esthetics. This analysis should be based on thorough cost and market estimations. However, since the cost estimation is outside the scope of this chapter, a traditional three-bladed rotor is assumed in this case.

3.5.6 Step 6: Choice of design lift and airfoils

As stated in Chapter 4, several different airfoils exist which can be used for wind turbine rotors. For this rotor, airfoils common in rotor design will be used: the NACA 63–4xx from relative thicknesses t/c = 15–21% and FFA-W3-xxx from relative thicknesses t/c = 24–36%. The airfoil characteristics are shown in Figs 3.13–3.16. When evaluating possible airfoils it is important

to know at which Reynolds numbers the blade will operate. As a rule of thumb, the Reynolds number will be between Re = 75 000R and 150 000R, which in this case, with R = 35 m, is between 2.6×10^6 and 5.3×10^6.

Wind tunnel measurements exist for most of the chosen airfoils. Measurements on the NACA 63–4xx airfoils are described by Abbott and Doenhoff.[20] They are measured at Re = 3×10^6 and 6×10^6. For this purpose Re = 6×10^6 has been chosen, because measurements with leading edge roughness (LER) also exist and because most of the energy will be produced for the airfoils operating at the higher end of the Reynolds number interval.

The FFA-W3-xxx airfoils are wind tunnel tested for only the 24% and 30% relative thickness. In addition, the existing wind tunnel tests have been carried out at Re = 1.6×10^6, so the design has to rely on measurements based on Reynolds numbers that are too low. Furthermore, data for leading edge roughness for the 30% airfoil is not available.

When analyzing the airfoil characteristics, much emphasis should be put on performance with leading edge roughness (LER), because the rotor will most probably frequently operate with dust and debris on the blade leading edge, which will reduce the airfoil efficiency.

It is obvious from Figs 3.13–3.17 that the computations by XFOIL do not predict the airfoil characteristics very well for the thick airfoils, whereas the predictions are quite good for the thinner airfoils. Even though uncertainties exist for wind tunnel data, considerable emphasis should be put on

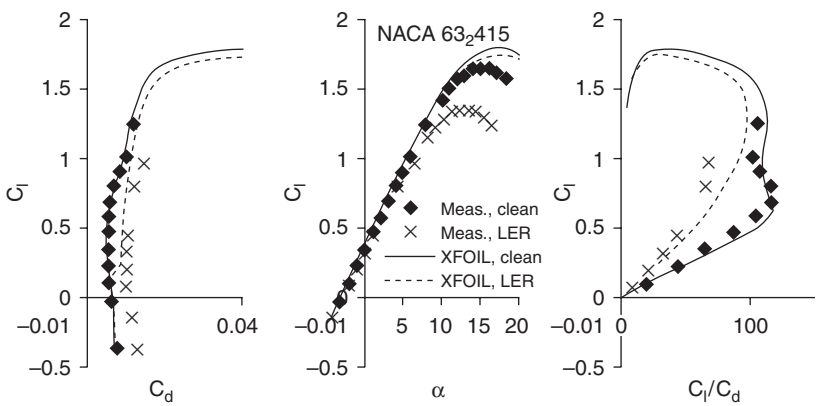

3.13 2D airfoil characteristics for NACA 63$_2$415 at Re = 6×10^6. (*Source*: Measurements from References 20 and 30). Computations using XFOIL. XFOIL,clean is free transition and XFOIL,LER is forced transition and computed according to the description in Chapter 4.

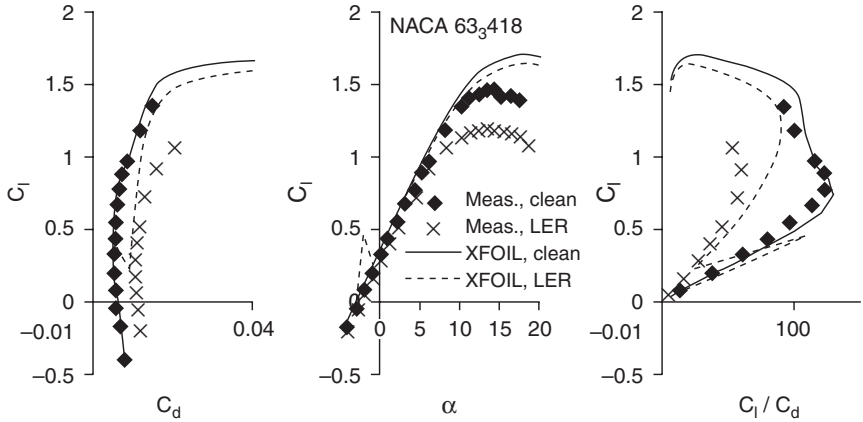

3.14 2D airfoil characteristics for NACA 63_3418 at Re = 6×10^6. (*Source*: Measurements from References 20 and 30). Computations using XFOIL. XFOIL,clean is free transition and XFOIL,LER is forced transition and computed according to the description in Chapter 4.

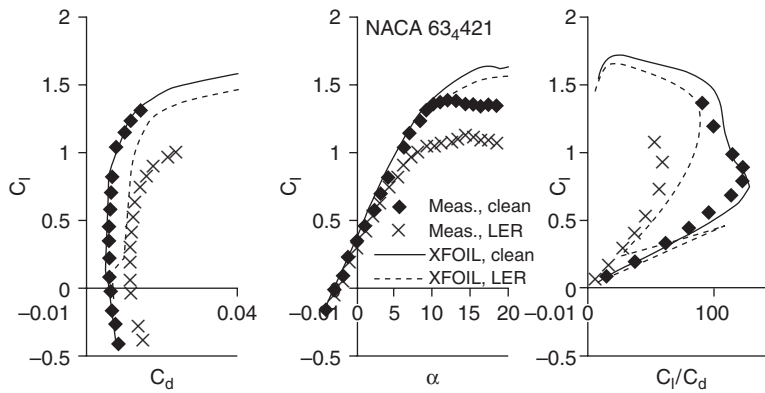

3.15 2D airfoil characteristics for NACA 63_4421 at Re = 6×10^6. (*Source*: Measurements from References 20 and 30). Computations using XFOIL. XFOIL,clean is free transition and XFOIL,LER is forced transition and computed according to the description in Chapter 4.

these data, because XFOIL and other flow simulation tools do not generally predict separated flows very accurately. However, if data are missing for airfoils, a rule of thumb is to simulate the airfoil performance assuming full turbulent flow, i.e. 'XFOIL, LER', to introduce a measure of conservatism and then use these data as a basis for the blade design.

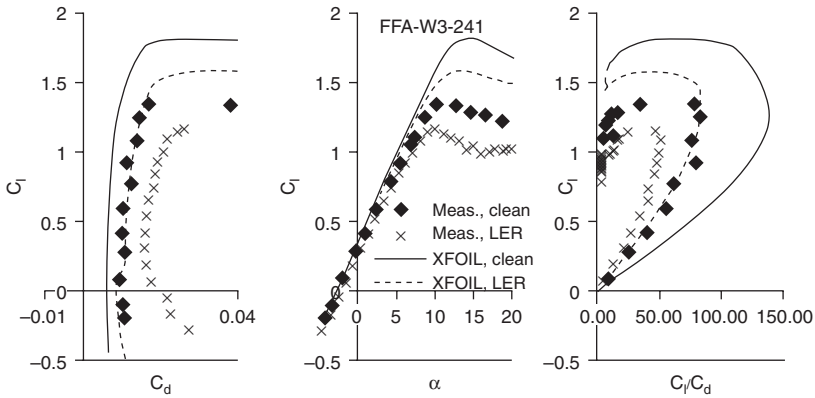

3.16 2D airfoil characteristics for FFA-W3-241 at Re = 1.6 × 10^6 for the measurements and Re = 6 × 10^6 for the computations. (*Source*: Measurements from References 30 and 31.) Computations using XFOIL. XFOIL,clean is free transition and XFOIL,LER is forced transition and computed according to the description in Chapter 4.

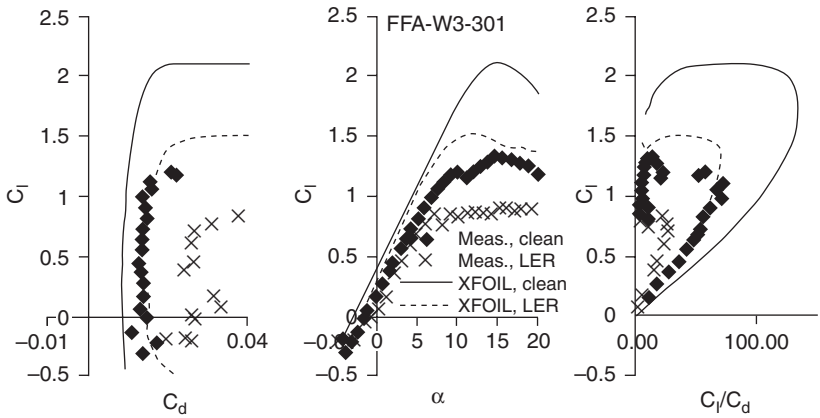

3.17 2D airfoil characteristics for FFA-W3-301 at Re = 1.6 × 10^6 for the measurements and Re = 6 × 10^6 for the computations. (Source: Measurements from References 30 and 31). Computations using XFOIL. XFOIL,clean is free transition and XFOIL,LER is forced transition and computed according to the description in Chapter 4.

The airfoil characteristics for the rotor should be used when the wind turbine performance is to be simulated at higher wind speeds. However, for the blade design process, the airfoil characteristics should be analyzed to find the lift coefficient used in the blade design, $c_{l,\text{design,blade}}$, and the

corresponding lift–drag ratio, $(c_l/c_d)_{\text{design,blade}}$, and angle of attack, $\alpha_{\text{design,blade}}$. Figures 3.18–3.20 show the distribution of these entities as a function of relative airfoil thickness, which will be used in the blade design process. These values are mainly based on the maximum lift from leading edge roughness measurements and reduced with Δc_l of approximately 0.4 to include a reserve in the operation, so that gusts or further reduction in maximum lift caused by even more severe leading edge roughness will not cause premature separation or stall. Thus, it should be noted that the lift coefficient used in the blade design, $c_{l,\text{design,blade}}$, ought to be equal to the lift coefficient for each airfoil for which the maximum lift–drag ratio exists, $c_{l,\text{design}}$. However, this is generally not possible because of the requirements of attached flow at all wind speeds. Since the data with leading edge roughness is based on severe contamination, the chosen design lift value is somewhat conservative and some designers would choose a higher design lift because this will result in a more slender blade, which again will result in reduced extreme and fatigue loads for the entire wind turbine. Another comment on the choice of $c_{l,\text{design,blade}}$ is, that it should be chosen so that the value is somewhere between the value measured or computed with clean surface and leading edge roughness, respectively, with the weight of, e.g. 70% clean surface and 30% leading edge roughness. This is to take into account the variations in blade surface quality over time.

As shown in Figs 3.18–3.20, it has been decided to describe the distribution of the entities using polynomial functions as trend lines because these are relatively smooth and easy to use. The smoothness of the functions will result in a smooth shaped blade. Other trend line functions exist and can

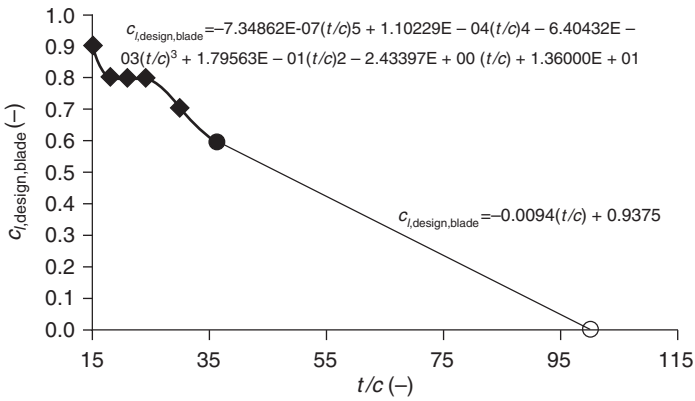

3.18 Distribution of $c_{l,\text{design,blade}}$ as a function of the relative thickness of the airfoil. A 5th order polynomial describes $c_{l,\text{design,blade}}$ from t/c = 15–36% and for t/c between 36% and 100% a linear relation is used as shown on the plot.

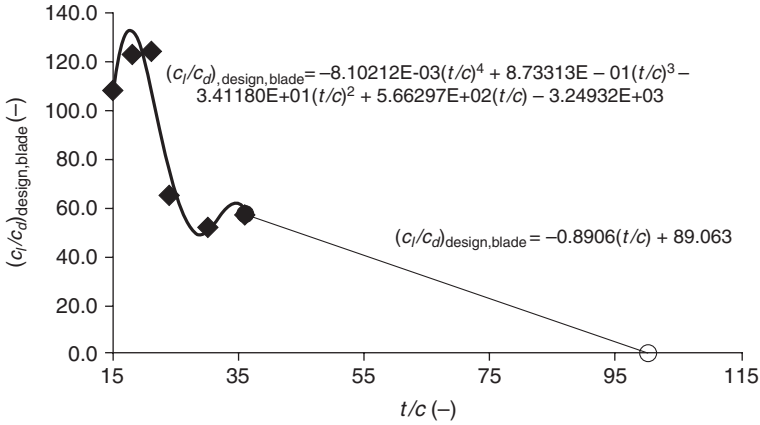

3.19 Distribution of $(c_l/c_d)_{design,blade}$ as a function of the relative thickness of the airfoil. A 4th order polynomial describes $(c_l/c_d)_{design,blade}$ from t/c = 15–36% and for t/c between 36% and 100% a linear relation is used as shown on the plot.

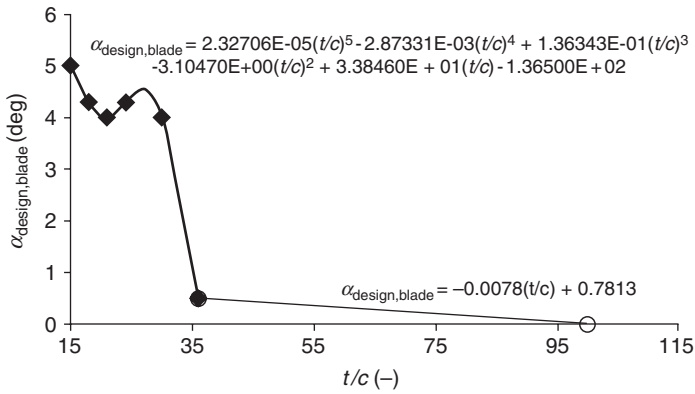

3.20 Distribution of $\alpha_{design,blade}$ as a function of the relative thickness of the airfoil. A 5th order polynomial describes $\alpha_{design,blade}$ from t/c = 15–36% and for t/c between 36% and 100% a linear relation is used as shown on the plot.

be used as well. Despite the relative smoothness of the functions they show abrupt changes between the 21% and 24% airfoil for the blade design lift–drag ratio distribution and between the 30% and 36% airfoil for the blade design angle-of-attack distribution. It should be noted that care should be taken to ensure that the smooth function is close to the actual values and that no under- or over-shoots of the function appear.

3.5.7 Step 7: Choice of design tip speed ratio

The choice of design tip speed ratio will in this case be simplified and, as previously mentioned, will be based only on maximizing the power coefficient C_P. No considerations concerning load reduction are to be taken into account. As a result of Step 6 it is known that the rotor operates with a lift–drag ratio for the thin airfoil sections of around 120. According to Fig. 3.9, a design TSR of 9 is appropriate for this lift–drag ratio to obtain maximum power efficiency.

3.5.8 Step 8: One point design of blade

In the previous steps, the basis of the blade design has been worked out. To summarize, we are now working on:

- a radius of 35 m,
- three blades,
- a maximum chord length of 3.0 m,
- a tip speed ratio of 9,
- a description of the blade design lift and the corresponding blade design angle of attack and blade design lift–drag ratio, and
- an estimated thickness distribution.

Based on this information, it is possible to design a blade in one point, i.e. at one tip speed ratio. Because the rotor is to operate with PRVS control this one point design will work well at low wind speeds, as long as the variable speed control is active. The planform is shown in Table 3.1 within the bolded lines, and the corresponding quantities are shown on the right of the table. In each column of the table a reference is found to the corresponding equation needed to describe the entity. The planform is plotted in Figs 3.21–3.23. In Fig. 3.21 it is noted that the root part, from around $r = 8$ m and inboards, has an uncommon shape. Often a transition area is needed from the airfoil part to a cylindrical part which will connect the blade to the hub and the pitch bearings. This is not taken into account in this design, where only the aerodynamic performance is in focus. However, this transition area should be corrected for in the final blade design.

3.5.9 Step 9: Evaluation of the blade design

The blade as designed in Step 8 should now be evaluated to reveal the aerodynamic performance, with power performance and load performance also being investigated, as well as the annual energy production. The aerodynamic

Table 3.1 Entities used in the blade design process. In each column there is a reference to an equation that describes the entity

R	c	θ	t/c	ϕ	$\alpha_{\text{design,blade}}$	f	F	a'	σ	c_x	c_y	$c_{l,\text{design,blade}}$	$(c_l/c_d)_{\text{design,blade}}$	λ_{loc}	t
	Equation [3.38]	Equation [3.16]		Equation [3.17]	Figure 3.20	Equation [3.26]	Equation [3.26]	Equation [3.31]	Equation [3.29]	Equation [3.23]	Equation [3.22]	Figure 3.18	Figure 3.19	Equation [3.35]	Figure 3.12
5.250	3.000	26.03	87.77	26.12	0.10	19.304	1.000	0.007	0.273	0.040	0.105	0.112	10.891	1.35	2.633
7.000	3.000	19.65	59.26	19.97	0.32	17.566	1.000	0.019	0.205	0.120	0.361	0.380	36.283	1.80	1.778
8.750	3.000	15.73	43.04	16.18	0.45	16.149	1.000	0.021	0.164	0.138	0.515	0.533	50.728	2.25	1.291
10.500	3.000	11.77	33.75	13.60	1.83	14.881	1.000	0.020	0.136	0.137	0.607	0.622	61.550	2.70	1.012
12.250	2.963	7.35	28.31	11.73	4.38	13.703	1.000	0.019	0.115	0.133	0.716	0.728	48.769	3.15	0.839
14.000	2.583	5.86	27.52	10.34	4.48	12.533	1.000	0.015	0.088	0.118	0.732	0.741	49.197	3.60	0.711
15.750	2.244	4.67	26.76	9.24	4.57	11.415	1.000	0.012	0.068	0.109	0.758	0.766	52.839	4.05	0.600
17.500	1.974	3.88	25.26	8.35	4.47	10.331	1.000	0.010	0.054	0.102	0.783	0.789	62.801	4.50	0.499
19.250	1.774	3.44	23.00	7.61	4.16	9.268	1.000	0.008	0.044	0.097	0.797	0.803	85.370	4.95	0.408
21.000	1.644	2.98	20.31	6.99	4.01	8.218	1.000	0.007	0.037	0.090	0.792	0.797	116.427	5.40	0.334
22.750	1.523	2.25	18.47	6.46	4.21	7.175	1.000	0.006	0.032	0.084	0.792	0.797	130.888	5.85	0.281
24.500	1.407	1.66	17.77	6.01	4.35	6.140	0.999	0.005	0.027	0.078	0.798	0.802	132.764	6.30	0.250
26.250	1.314	1.28	17.84	5.62	4.34	5.110	0.996	0.004	0.024	0.072	0.798	0.801	132.693	6.75	0.234
28.000	1.230	1.01	18.19	5.27	4.26	4.083	0.989	0.004	0.021	0.067	0.795	0.798	131.929	7.20	0.224
29.750	1.136	0.67	18.05	4.96	4.29	3.059	0.970	0.003	0.018	0.063	0.797	0.799	132.306	7.65	0.205
31.500	0.992	0.12	16.86	4.69	4.57	2.038	0.917	0.003	0.015	0.061	0.816	0.818	130.863	8.10	0.167
33.250	0.720	–0.53	15.00	4.45	4.98	1.018	0.765	0.003	0.010	0.061	0.889	0.891	108.681	8.55	0.108
34.125	0.536	–0.67	15.00	4.33	5.00	0.509	0.589	0.003	0.007	0.060	0.898	0.900	105.847	8.78	0.074
34.983	0.120	3.49	35.50	4.23	0.74	0.010	0.091	0.002	0.002	0.034	0.601	0.602	60.019	9.00	0.043

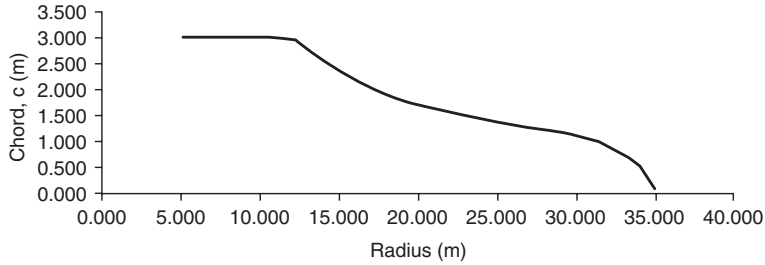

3.21 Chord distribution.

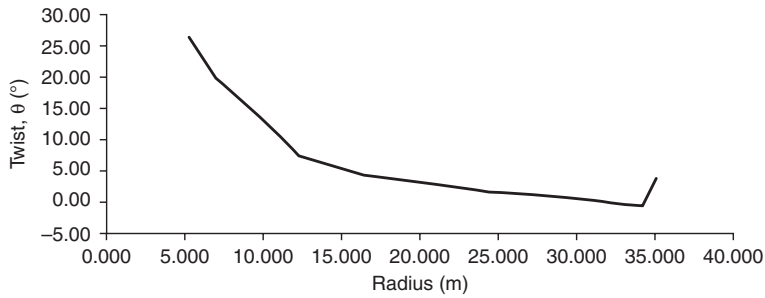

3.22 Twist distribution.

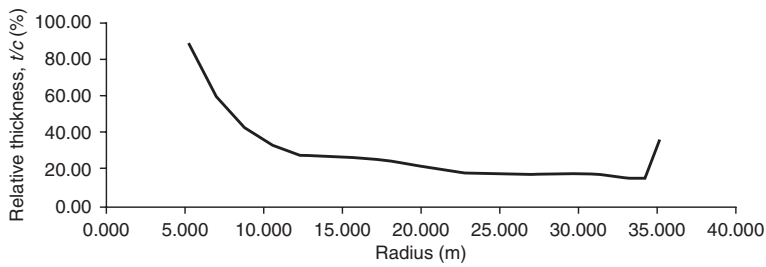

3.23 Relative thickness distribution.

tool HAWTOPT,[2] developed at DTU Wind Energy, Denmark, will be used. However, before commencing the evaluation, the airfoil characteristics should be corrected for three-dimensional flow effects such as centrifugal and Coriolis forces, which appear when the flow starts to separate. For this purpose, the models mentioned in Chapter 4 can be used. In general, these corrections will increase the maximum lift the closer the airfoil sections are to the hub. The corrections are important for precise estimation of the rotor performance for the PRVS concept, but because most of the rotor experiences attached flow in normal operation the influence of the 3D effects are

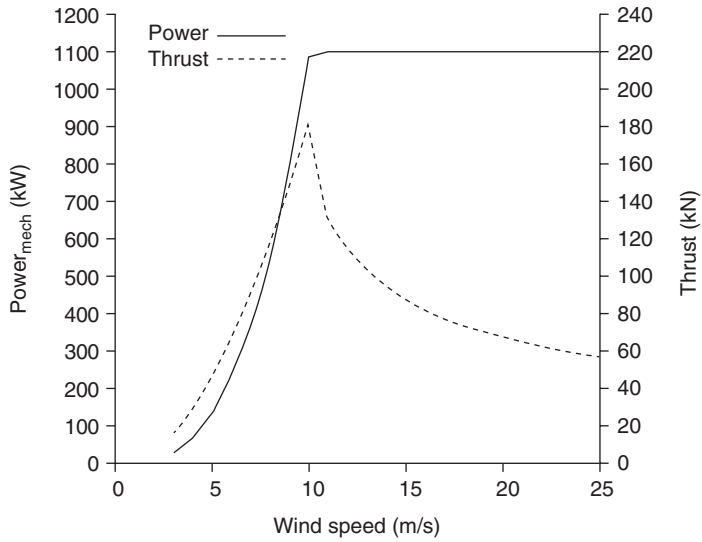

3.24 Mechanical power and thrust as a function of wind speed – so-called power and thrust curves.

fairly small. However, if a rotor for a stall regulated turbine were designed, the rotor would experience, for high wind speeds, separated flow on the entire rotor, and the 3D corrections would be crucial for making fair predictions of power and loads. In this example the 3D correction model by Bak *et al.*[32] is used.

The power without drivetrain losses and the thrust are shown in Fig. 3.24 assuming a drivetrain loss of approximately 10%. In addition, Fig. 3.25 shows the corresponding rotational speed and pitch. It can be seen that the rated power obtained is slightly above a wind speed of 10 m/s and not 12 m/s as estimated. This might be due to a relatively optimistic power curve, where the power at the 'knee' of the power curve is not obtainable in a real turbine because of the fast changes in the pitch curve at these wind speeds. However, consideration should be given to whether the rotor is the right size in relation to the generator to obtain minimum cost of energy. For this purpose, it is important to predict the annual energy production (AEP). With the given control settings and on the given site AEP = 2270 MWh. Relating AEP to the number of hours in a year, the mean mechanical power for the rotor in this wind climate is 259 kW. This is 25.9% of the rated power, which agrees well with the rule of thumb of 25% for traditional wind turbine rotors. However, the trend for the newest rotor designs is that this value is increasing up to 30% and even 40%, which corresponds to the trend of increasing rotor diameters for fixed generator size.

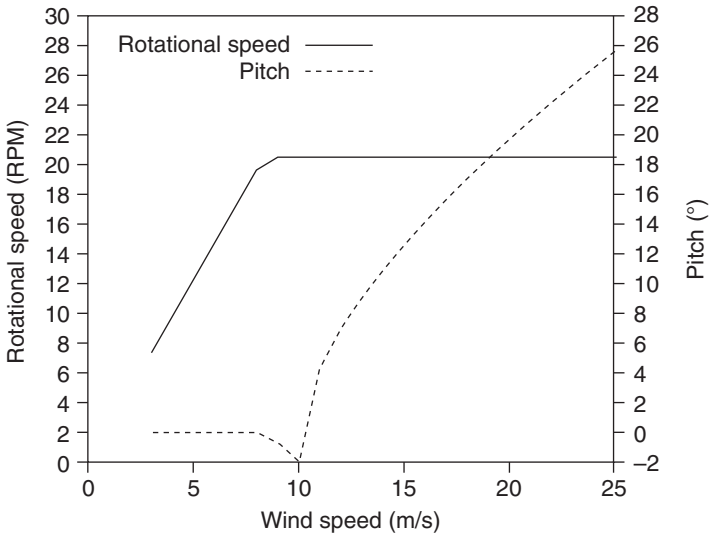

3.25 Rotational speed and pitch as a function of wind speed.

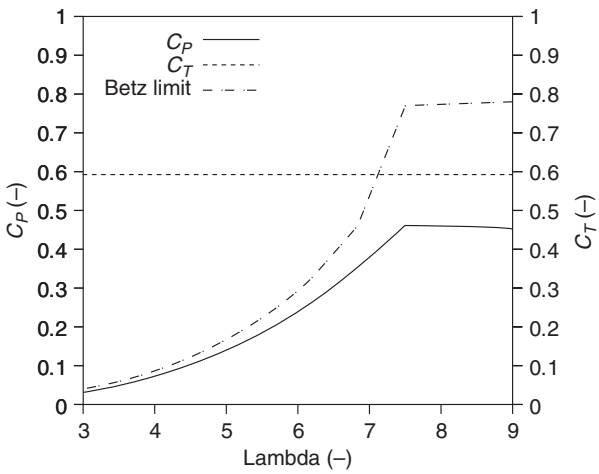

3.26 Power and thrust coefficient as a function of tip speed ratio λ. Also, the Betz limit is shown.

Figure 3.26 shows the power coefficient and the thrust coefficient. It is noted that the power coefficient is somewhat below the Betz limit. Analyzing this, Fig. 3.27 shows the local power and thrust coefficient, reflecting how the efficiency is distributed along the blade at a wind speed of 8 m/s. In terms of the power coefficient, the blade is rather inefficient on the inner part of the blade, especially from r = 12 m and inboards. This is partly due to

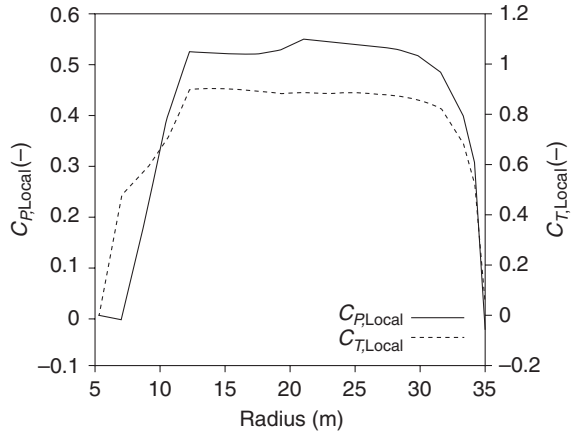

3.27 Local mechanical power and thrust coefficient as a function of rotor radius at a wind speed of 8 m/s corresponding to $\lambda = 9.0$.

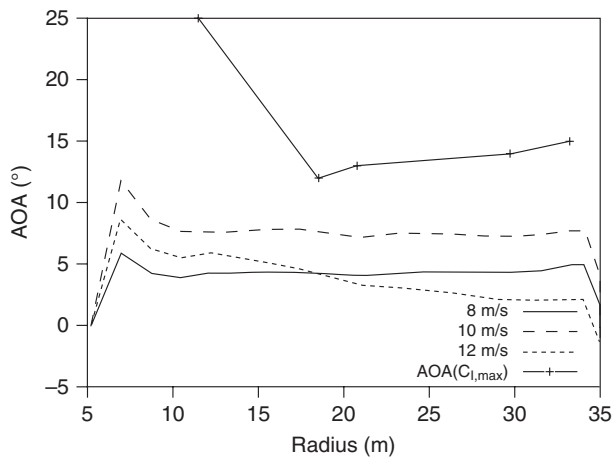

3.28 Angle of attack as a function of radius.

the conservatism in the airfoil characteristics for the FFA-W3-xxx airfoils (which were measured at a lower Reynolds number than the number at which the rotor actually operates). In addition, a negative power coefficient is seen at the tip and at the root, which is due to the thick airfoil section of 35.5% relative thickness at the tip and the relative thickness of approximately 60% close to the root.

To ensure that the rotor will not produce too much noise and possibly lose power, the angle of attack during operation should be investigated. This is shown in Fig. 3.28 for the case of mean wind speeds. The corresponding

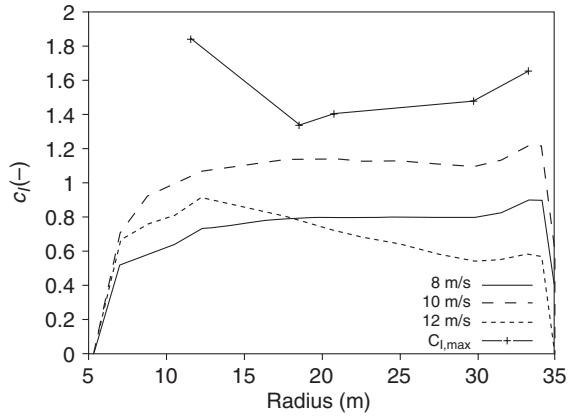

3.29 Lift coefficient as a function of radius.

lift coefficient, c_l, is shown in Fig. 3.29. However, gusts entering the rotor will result in a sudden increase in the angle of attack, potentially causing separation and corresponding noise and loss of power. Thus, even though Figs 3.28 and 3.29 show that the operation at a wind speed of 10 m/s is closest to maximum lift and that the rotor, even at this wind speed, will be free of separation and far from maximum lift, the performance, i.e. load, power and risk of separation, should be investigated using an aeroelastic code which uses the relevant wind climate parameters in terms of turbulence intensity and the Weibull distribution for which it is designed.

Figure 3.30 shows the Reynolds numbers as a function of radius at wind speeds from 8 to 12 m/s. At 8 m/s the rotor is still operating in the variable speed range, but at 10 and 12 m/s maximum rotational speed is obtained. It shows that the Reynolds numbers used from the wind tunnel tests correspond fairly well for the 18% and 21% relative thickness, with a maximum $Re = 5 \times 10^6$ on the blade compared to $Re = 6 \times 10^6$ in the tunnel. However, for the thicker airfoils, $Re = 1.6 \times 10^6$ as measured in the tunnel, is too low compared to the $Re = 5 \times 10^6$ on the blade. For the 15% airfoil the blade seems to operate at $Re = 3 \times 10^6$ on the blade, whereas $Re = 6 \times 10^6$, was used in the design process.

Analyzing the geometry of the blade planform, the chord distribution is relatively smooth and should cause no significant problems when creating the structure. However, the twist and the distribution in relative thickness are not as smooth, and so some adjustments might be necessary to allow the distribution of the different parameters to be smooth and to allow them to change continuously. Finally, the structural design should be analyzed for potential improvements concerning, e.g. strength, stress, strain and manufacturing process.

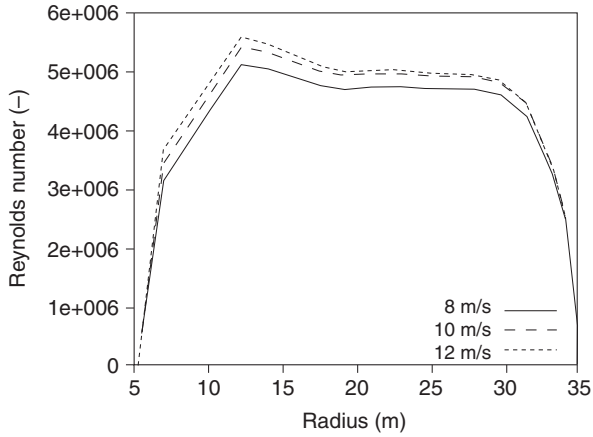

3.30 Reynolds number as a function of radius.

Using this (Step 9) evaluation of the design, a new iteration in the blade design process is carried out starting from the step at which the findings in the evaluation influence the design for the first time in the process. For the above design, new airfoil characteristics for $t/c = 15\%$ and for $t/c \geq 24\%$ should be obtained because they seem to affect the design too much. Therefore a new iteration in the rotor design process should be carried out starting at Step 6. However, if an aeroelastic code were used to show the load response from the entire wind turbine and if a proper cost function were set up, a new iteration in the rotor design process could start at an even earlier step, possibly beginning at Step 2, scaling the rotor diameter.

3.6 Future trends

With the increasing volume of wind turbines on the world market and the increasing interest in wind energy that is in evidence in 2013, it seems that several development lines in rotor design will be followed. One line is a new market for small wind turbines in the kW range. Many different concepts are being tested, as was the case at the end of the 1970s and in the early 1980s, and so for this size of rotor, the trend is not yet clear. Another line of development is the large MW wind turbine, which is based on experience gained in the early 1980s and up-scaling of concepts from that time.

As far as blade design for MW wind turbines is concerned, different shapes exist at the moment. The differences in shape relate to the degree of load reduction that is required. Some blades are designed with rather thin relative thickness of the airfoil sections from tip to root, and quite large chord lengths are allowed. Other blades are designed with large relative

thickness of the airfoil sections close to the root, with a transition area from the airfoil sections to a cylinder part and a correspondingly small allowable maximum chord length. This difference is due to the load predictions for the entire wind turbine in certain conditions, e.g. with the rotor idling in extreme wind. During recent years, there has been a trend towards slender blades to reduce the loads on the entire turbine. This type of design is often combined with quite a large rotor compared to the generator size in order to increase the swept area and thereby the power. Another way to reduce loads is to equip the blades with trailing edge flaps, so that they can actively reduce fluctuating loads. This technique is being developed and has been investigated for use on wind turbines since 2003.[33–37] Increased use of sensors will probably also affect blade design with strain gauges and accelerometers being embedded in the blade for control or condition monitoring or laser measurements upstream of the rotor, e.g. the Wind Scanner[38] which is used for control of the rotor.

With the increasing volume of wind turbines on the market it seems increasingly cost-effective to design wind turbines and rotors for specific wind climates. Various aspects therefore need to be considered, such as whether the turbine is to be erected offshore or in complex terrain and whether it is to be erected on low wind sites or high wind sites. There is a trend towards designing turbines and rotors which are specialized for particular sites.

Irrespective of whether they are designed with large or small maximum chord lengths close to the root, there is a trend towards making blades more aerodynamically efficient. Especially as regards the inner part of the blade, where thick airfoils are used, much effort is put into the understanding and correct modeling of this part of the rotor, where high thrust close to the root has been observed to result in suction of the flow through the rotor because of swirl in the wake close to the hub.[39] Thus, more focus on thicker airfoils, and new concepts relating to the rotor aerodynamics of the inner part of the rotor, will probably be seen.[40]

3.7 Sources of further information and advice

The design of rotors requires the use of different tools. In particular, the mechanisms that cannot be described by the Blade Element Momentum (BEM) method have been the subject of research since the 1980s, and, more recently, advanced tools such as Computational Fluid Dynamics have proved very useful. Wind tunnel tests on rotors have been carried out[41,42] and rotor tests in atmospheric flow have also been carried out.[43–46] Recently an experiment on a rotor for a 2.3 MW modern wind turbine was carried out, measuring both pressure distributions on the blade surface and fast pressure fluctuations up to 10 kHz in order to investigate the smallest eddies in the

turbulence characteristics around wind turbine blades in operation.[47,48] Also, Siemens have carried out full scale experiments on a 2.3 MW wind turbine, measuring the aerodynamic performance.[49] In addition to these recent full scale tests, details of the aerodynamic rotor design have been investigated at different research institutions such as NREL (USA), UC Davis (USA), ECN (The Netherlands), Delft (The Netherlands), Stuttgart (Germany), FOI (Sweden) and finally DTU MEK and Risø National Laboratory (Denmark) (now merged and called DTU Wind Energy). Overviews of aerodynamic rotor design have been given by Tangler[50] and Snel.[51]

3.8 Acknowledgements

I wish to thank my colleagues at DTU Wind Energy, Denmark, particularly the Aeroelastic Design Section, which is a continuous source of inspiration. I especially wish to thank Mac Gaunaa, Flemming Rasmussen and Frederik Zahle from the Aeroelastic Design Program for fruitful discussion.

3.9 References

1. BTM Consult ApS, 'International Wind Energy Development. World Market Update 2011. Forecast 2012–2016', BTM Consult, March 2012.
2. Fuglsang, P., Thomsen, K., Site-specific design optimization of 1.5–2.0 MW wind turbines. *J. Solar Energy Eng*., **123**, 296–303, 2001.
3. Xudong, W., Shen, W.Z., Zhu, W.J., Sørensen, J.N., Jin, C., Shape optimization of wind turbine blades. *Wind Energy*, **12**(8), 781–803, 2009.
4. ANSYS Fluent, www.ansys.com
5. ANSYS CFX, www.ansys.com
6. STAR-CD, www.cd-adapco.com
7. Michelsen J.A. Basis3d – a platform for development of multiblock pde solvers. Technical report afm 92–05, Technical University of Denmark, 1992.
8. Michelsen J.A. Block structured multigrid solution of 2d and 3d elliptic pde's. Technical report afm 94–06, Technical University of Denmark, 1994.
9. Sørensen N.N. General purpose flow solver applied to flow over hills. Risø-r-827(en), Risø National Laboratory, Denmark, June 1995.
10. Johansen, J., Madsen, H.Aa., Gauna, M., Bak, C., Sørensen, N.N., Design of a wind turbine rotor for maximum aerodynamic efficiency. *Wind Energy,* **12**(3), 261–273, 2009.
11. Sørensen, J.N., Shen, W.Z., Numerical modelling of Wind Turbine Wakes. *Journal of Fluids Engineering*, **124**(2), 393–399, 2002.
12. Mikkelsen, R., Actuator Disc Methods Applied to Wind Turbines, MEK-FM-PHD 2003–02, Technical University of Denmark, 2003.
13. Madsen, H.A., 'A CFD analysis of the actuator disc flow compared with momentum theory results', 10th IEA meeting on Aerodynamics, University of Edinburgh, 16–17 December 1996.
14. Voutsinas, S.G., Riziotis, V.A., Vortex particle modeling of stall on rotors. Application to wind turbines. Proceedings of the Fluids Engineering Division Summer Meeting, ASME, San Diego, 1996.

15. Glauert, H., Airplane Propellers. *Aerodynamic Theory Volume **IV*** edited by William Frederick Durand. The Dover edition 1963.
16. Wilson, R.E., Lissaman, P.B.S., Applied aerodynamics of wind power machines. Oregon State University. May 1974.
17. Andersen, P.S., Krabbe, U., Lundsager, P., Petersen, H., 'Basismateriale for Beregning af Propelvindmølle', Risø-M-2153(rev.), Risø, Januar, 1980 (in Danish).
18. Hansen., M.O.L., *Aerodynamics of Wind Turbines*, 2nd edition, Earthscan, 2008.
19. Prandtl, L., Betz, A., 'Schraubenpropeller mit geringstem Energieverlust', Göttinger Nachrichten, 1919.
20. Abbott, I.H., Doenhoff, A.E.von, *Theory of Wing Sections*, Dover Publications, 1959.
21. Bak, C., 'Sensitivity of key parameters in aerodynamic wind turbine rotor design on power and energy performance', Proc. The Science of Making Torque from Wind, *Journal of Physics: Conference Series*, **75**, 012008, 2007.
22. Brooks, T.F., Pope, D.S., Marcolini, M.A., *Airfoil Self-Noise and Prediction*, NASA Reference Publication 1218, USA, 1989.
23. Øye, S., 'FLEX 4 – Simulation of Wind Turbine Dynamics', Proceedings of the 28th IEA Meeting of Experts 'State of the Art of Aeroelastic Codes for Wind Turbine Calculations', pp. 71–76, Technical University of Denmark, Lyngby, Denmark, 11–12 April 1996.
24. Bossanyi, E.A., *GH-Bladed User Manual*, Issue 14, Garrad Hassan and Partners Limited, Bristol, UK, 2004.
25. Lindenburg, C., Schepers, J.G., 'Phatas-IV Aero-elastic Modelling, Release' DEC-1999 and NOV-2000, ECN-CX – 00–027, 2000.
26. Jonkman, J.M., Buhl, Jr., M.L., *FAST User's Guide*, NREL/EL-500–29798, Golden, CO: National Renewable Energy Laboratory, 2005.
27. Larsen, T.J., Madsen, H.A., Hansen, A.M., Thomsen, K. Investigations of stability effects of an offshore wind turbine using the new aeroelastic code HAWC2. Proceedings of the conference, 'Copenhagen Offshore Wind 2005', 2005.
28. International Standard, IEC 61400-1 Edition 3.0, Wind turbines – Part 1: Design requirements, www.iec.ch
29. Troen, I., Lundtang, E.L., *European Wind Atlas*, Risø National Laboratory, Roskilde, Denmark.
30. Bertagnolio, F., Sørensen, N.N., Johansen, J., Fuglsang, P., Wind turbine airfoil catalogue. Risø-R-1280(EN), 151 p, 2001.
31. Fuglsang, P., Antoniou, I., Dahl, K.S., Madsen, H.A., 'Wind Tunnel Tests of the FFA-W3–241, FFA-W3–301 and NACA 63–430 Airfoils', Risø-R-1041(EN), Risø National Laboratory, Roskilde, Denmark, December 1998.
32. Bak, C., Johansen, J., Andersen, P.B., Three-Dimensional Corrections of Airfoil Characteristics Based on Pressure Distributions, Proc. European Wind Energy Conference & Exhibition (EWEC), 27 February–2 March 2006, Athens, Greece.
33. Buhl, T., Gaunaa, M., Bak, C., 'Potential load reduction using airfoils with variable trailing edge geometry', *Journal of Solar Energy Engineering*, **127**, 503–516, November 2005.
34. Andersen, P.B., Henriksen, L., Gaunaa, M., Bak, C., Buhl, T., Deformable trailing edge flaps for modern megawatt wind turbine controllers using strain gauge sensors, *Wind Energy*, **13**(2–3), 193–206, 2009.

35. Barlas, A., Kuik, G.A.M. van, 'State of the art and prospectives of smart rotor control for wind turbines', In the Proceedings of The Science of Making Torque from Wind, Lyngby, Denmark, August 28–31, 2007.
36. Yen Nakafuji, D., van Dam, C., Smith, R., Collins, S., 'Active load control for airfoils using microtabs', *J. Sol. Energy Eng*., **123**, 282–289, 2001.
37. Castaignet, D., 'Model predictive control of trailing edge flaps on a wind turbine blade', PhD thesis, Technical University of Denmark, National Laboratory for Sustainable Energy, Wind Energy Department Roskilde, November 2011.
38. Mikkelsen, T., Mann, J., Courtney, M., Sjöholm, M., 'Windscanner: 3-D wind and turbulence measurements from three steerable doppler lidars', 14th International Symposium for the Advancement of Boundary Layer Remote Sensing, Earth and Environmental Science, **1**, 2008.
39. Johansen, J., Madsen, H.Aa., Gaunaa, M., Bak, C., Sørensen, N., 'Design of a wind turbine rotor for maximum aerodynamic efficiency', *Wind Energy*, **12**(3), s. 261–273, 2009.
40. Zahle, F., Gaunaa, M., Sørensen, N.N., Bak,C., 'Design and wind tunnel testing of a thick, multi-element high-lift airfoil', Proc. EWEA 2012 – European Wind Energy Conference & Exhibition, Copenhagen, Denmark, 16–19 April 2012.
41. Hand, M.M., Simms, D.A., Fingersh, L.J., Jager, D.W., Cotrell, J.R., Schreck, S., Larwood, S.M., 'Unsteady Aerodynamics Experiment Phase VI: Wind Tunnel Test Configurations and Available Data Campaigns', NREL/TP-500–29955, National Renewable Energy Laboratory, Golden, Colorado, USA, December 2001.
42. Snel, H., Schepers, J.G., Montgomerie, B., The MEXICO project (Model Experiments in Controlled Conditions): The database and first results of data processing and interpretation, Proc. The Science of Making Torque from Wind, *Journal of Physics: Conference Series*, **75**, 012014, 2007.
43. Madsen, H.A., Petersen, S.M. 'Wind turbine test Tellus T-1995, 95 kW', *Risø-M-2761*, Risø National Laboratory, Roskilde, 1989.
44. Brand, A.J., Dekker, J.W.M., de Groot, C.M., Spath, M., 'Field rotor aerodynamics: the rotating case', ECN-RX – 96–067, ECN, 1996.
45. Simms, D.A., Fingersh, L.J., Butterfield, C.P., 'NREL Unsteady Aerodynamics Experiment Phase III Test Objectives and Preliminary Results', Wind Energy 1995: Proceedings of the Energy and Environmental Expo '95, the Energy-Sources Technology Conference and Exhibition, 29 January–1 February 1995, Houston, Texas. SED-Vol. **16**, pp. 273–275.
46. Schepers, J.G., Brand, A.J., Bruining, A., Graham, J.M.R., Hand, M.M., Infield, D.G., Madsen, H.A., Paynter, R.J.H., Simms, D.A., Final report of IEA Annex XIV: Field Rotor Aerodynamics, ECN-C – 97–027, Netherlands Energy Research Foundation, May 1997.
47. Madsen, H.A., Bak, C., Paulsen, U.S., Gaunaa, M., Fuglsang, P., Romblad, J., Olesen, N.A., Enevoldsen, P., Laursen, J., Jensen, L., 'The DAN-AERO MW Experiments. Final report', Risø-R-1726(EN), ISSN 0106–2840, ISBN 978-87-550-3809-7, Risø National Laboratory for Sustainable Energy, Technical University of Denmark, Roskilde, Denmark, September 2010.
48. Bak, C., Madsen, H.A., Paulsen, U.S., Gaunaa, M., Fuglsang, P., Romblad, J., Olesen, N.A., Enevoldsen, P., Laursen, J., Jensen, L., 'DAN-AERO MW: Detailed aerodynamic measurements on a full scale MW wind turbine', Proc. 2010 European Wind Energy Conference and Exhibition, Warsaw, Poland, 20–23 April 2010.

49. Medina, P., Singh, M., Johansen, J., Jove, A.R., Machefaux, E., Fingersh, L.J., Schreck, S., 'Aerodynamic and Performance Measurements on a SWT-2.3–101 Wind Turbine', WINDPOWER 2011 Anaheim, California, 22–25 May 2011.
50. Tangler, The Evolution of Rotor and Blade Design, Presented at the American Wind Energy Association WindPower 2000, Palm Springs, California, 30 April–4 May 2000.
51. Snel, H., 'Review of aerodynamics for wind turbines', *Wind Energy*, **6**, 203–211, 2003.

3.10 Appendix: Nomenclature

Symbol	Unit	Description
a	-	Induced axial velocity in rotor plane
a'	-	Induced tangential velocity in rotor plane
A	m^2	Area of rotor plane
A_h	m/s	Parameter in Weibull distribution relating to the mean wind speed
B	-	Number of blades on rotor
c	m	Chord length or distance from very leading edge to very trailing edge of airfoil
c_d	-	Drag coefficient
c_l	-	Lift coefficient
$c_{l,\text{design}}$	-	Lift coefficient at which $(c_l/c_d)_{\text{design}}$ is obtained (design lift)
$c_{l,\text{design,blade}}$	-	Lift coefficient used to design the blade (blade design lift)
$c_{l,\text{max}}$	-	Maximum lift coefficient
c_l/c_d	-	Lift–drag ratio
$(c_l/c_d)_{\text{design}}$	-	Maximum lift–drag ratio for airfoil section
$(c_l/c_d)_{\text{design,blade}}$	-	Lift–drag ratio at which $c_{l,\text{design,blade}}$ is obtained
c_x	-	Force coefficient on airfoil driving the rotor – parallel to rotor plane
c_y	-	Force coefficient on airfoil contributing to rotor thrust – orthogonal to rotor plane
C_P	-	Rotor power coefficient
C_T	-	Rotor thrust coefficient
D	N	Drag on airfoil
f	-	Exponent in the Prandtl tip correction formula
F	-	Prandtl tip correction
$F_{\text{tangential}}$	N/m	Force per length unit in tangential direction on an airfoil section
h	m	Height above ground at which the wind speed will be modeled
h_{measured}	m	Height above ground at which the wind speed is measured (commonly 10 m)
H	Pa	Stagnation pressure
k_h	-	Parameter in the Weibull distribution
$k_{h,\text{measured}}$	-	Parameter in the Weibull distribution determined from measurements
L	N	Lift on airfoil
p	Pa	Pressure in the rotor plane on the upstream side

Symbol	Unit	Description
p_0	Pa	Pressure far upstream and downstream of the rotor
P	W	Mechanical power from the rotor
P_{wind}	W	Power available from the wind
Q	Nm	Torque from the rotor
r	m	Radius locally on the blade
R	m	Tip radius
Re	-	Reynolds number
t	m	Maximum thickness of airfoil measured orthogonal to the chord
T	N	Thrust on rotor
T_{wind}	N	Thrust from the wind
TSR	-	Tip Speed Ratio = λ
u	m/s	Wind speed in the rotor plane
u_1	m/s	Wind speed far downstream in the rotor wake
V_0	m/s	Wind speed far upstream of the rotor
W	m/s	Relative velocity on the airfoil which is the combination of the axial and the tangential inflow
z_0	m	Terrain roughness length
α	°	Angle of attack
α_{design}	°	Angle of attack at which $c_{l,design}$ is obtained
$\alpha_{design,blade}$	°	Angle of attack at which $c_{l,design,blade}$ is obtained
Δp	Pa	Pressure jump over the rotor disc
ϕ	°	Angle between the relative inflow and the rotor plane
λ_{loc}	-	Ratio between the local tangential velocity of the rotor and the wind speed far upstream
λ	-	Ratio between the tangential velocity at the tip of the rotor and the wind speed far upstream (tip speed ratio)
ν	m^2/s	Air dynamic viscosity
ω	rad/s	Rotational speed of the rotor
ρ	kg/m^3	Air density
σ	-	Solidity of the rotor
θ	°	Pitch angle